AD-A042 528 ROCKWELL INTERNATIONAL THOUSAND OAKS CALIF SCIENCE --ETC F/G 11/4
STRUCTURAL DEGRADATION IN FIBER COMPOSITES BY KINKING.(U)
MAY 77 A G EVANS, W F ADLER N00014-76-C-0854

UNCLASSIFIED SC5076.3TR NL

| OF |
AD
A042528

END
DATE
FILMED
8-77
DDC

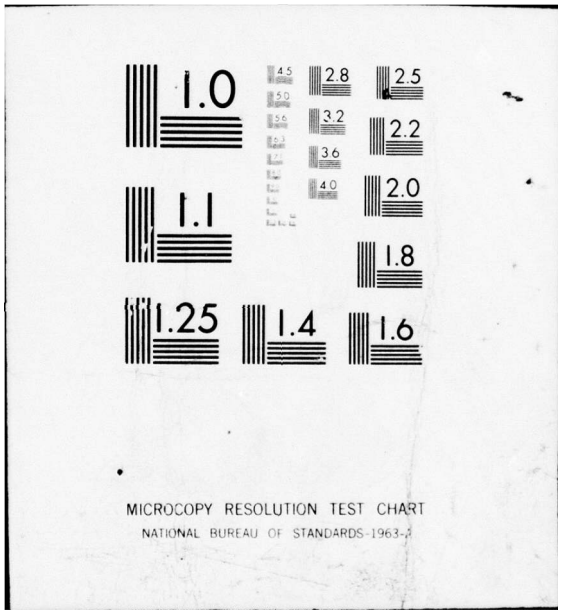
1.0
1.1
1.25
1.4
1.6
1.8
2.0
2.2
2.5
2.8
3.2
3.6
4.0
4.5
5.0
5.6
6.3
MICROCOPY RESOLUTION TEST CHART
NATIONAL BUREAU OF STANDARDS-1963-A

12

SC5076.3TR

COPY NO. 16

STRUCTURAL DEGRADATION IN FIBER COMPOSITES BY KINKING

TECHNICAL REPORT

May 1, 1976 thru April 30, 1977
Contract No. N00014-76-C-0854

Submitted to:

Office of Naval Research
800 N. Quincy Street
Arlington, VA 22217

This Research was Sponsored by the Office of Naval Research
Under Contract No. N00014-76-C-0854 (Project No. 471)

Science Center
Rockwell International

Unclassified

SECURITY CLASSIFICATION OF THIS PAGE *(When Data Entered)*

REPORT DOCUMENTATION PAGE		READ INSTRUCTIONS BEFORE COMPLETING FORM
1. REPORT NUMBER	2. GOVT ACCESSION NO.	3. RECIPIENT'S CATALOG NUMBER
4. TITLE *(and Subtitle)* (6) STRUCTURAL DEGRADATION IN FIBER COMPOSITES BY KINKING, (14)		5. TYPE OF REPORT & PERIOD COVERED Technical Report May 1, 1976 thru April 30, 1977
		6. PERFORMING ORG. REPORT NUMBER SC5076.3TR
7. AUTHOR(s) (10) A. G. Evans and W. F. Adler		8. CONTRACT OR GRANT NUMBER(s) (15) N00014-76-C-0854
9. PERFORMING ORGANIZATION NAME AND ADDRESS Rockwell International Science Center Thousand Oaks, CA 91360		10. PROGRAM ELEMENT, PROJECT, TASK AREA & WORK UNIT NUMBERS Project No. 471 (NR032-570)
11. CONTROLLING OFFICE NAME AND ADDRESS Office Of Naval Research 800 N. Quincy Street Arlington, VA 22217 (12) 62 p.		12. REPORT DATE (11) May 1, 1977
		13. NUMBER OF PAGES 53
14. MONITORING AGENCY NAME & ADDRESS *(if different from Controlling Office)*		15. SECURITY CLASS. *(of this report)* Unclassified
		15a. DECLASSIFICATION/DOWNGRADING SCHEDULE

16. DISTRIBUTION STATEMENT *(of this Report)*

Approved for Public Release; distribution unlimited

Technical rpt. 1 May 76–30 Apr 77

17. DISTRIBUTION STATEMENT *(of the abstract entered in Block 20, if different from Report)*

18. SUPPLEMENTARY NOTES

19. KEY WORDS *(Continue on reverse side if necessary and identify by block number)*

Compressive fracture, kinking, carbon/carbon composites, fiber fracture, matrix yield strength, impact damage, erosion

20. ABSTRACT *(Continue on reverse side if necessary and identify by block number)*

Some observations of kinking in carbon composites, which identify the modes and morphology of kinking in fibrous materials, are presented. The thermodynamics and mechanics of kinking are analyzed. The analyses indicate the important role of matrix deformation (plastic and elastic) in determining the kink morphology, and identify the matrix yield strength and the distribution of fiber fracture strengtns as the primary properties governing kink formation.

DD FORM 1 JAN 73 1473 EDITION OF 1 NOV 65 IS OBSOLETE

Unclassified 389 949

SECURITY CLASSIFICATION OF THIS PAGE *(When Data Entered)*

SC5076.3TR

STRUCTURAL DEGRADATION IN FIBER COMPOSITES BY KINKING

Technical Report
for the period 05/01/76 thru 04/30/77

GENERAL ORDER NO. 5076

CONTRACT NO. N00014-76-C-0854

Project No. 471 (NR032-570)

Prepared for:

Office of Naval Research
800 North Quincy Street
Arlington, VA 22217

by

A. G. Evans

Science Center, Rockwell International
Thousand Oaks, California 91360

and

W. F. Adler

Effects Technology, Inc.
Santa Barbara, California 93111

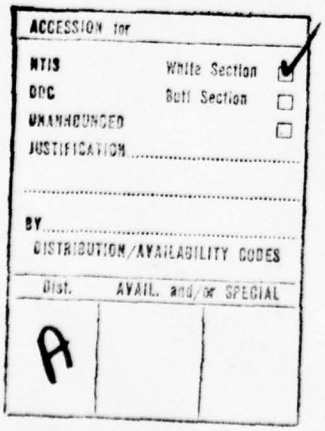

Science Center
Rockwell International
1049 CAMINO DOS RIOS
THOUSAND OAKS, CALIF. 91360
805/498 4545

TABLE OF CONTENTS

			Pg.
1.0	INTRODUCTION		1
2.0	EXPERIMENTAL		
	2.1	Materials and Test Methods	2
	2.2	Kink Observations	3
	2.3	Micromechanics Tests	4
3.0	THERMODYNAMIC ANALYSIS		5
	3.1	Kink Morphology	6
	3.1.1	Plastic Work	8
	3.1.2	Kink Formation	11
4.0	MECHANICS OF KINKING		13
	4.1	"Shear" Kinks	13
	4.2	Compressional Kinks	18
5.0	IMPLICATIONS AND CONCLUSIONS		20
APPENDIX I			22
APPENDIX II			25
REFERENCES			28
FIGURE CAPTIONS			29

ABSTRACT

Some observations of kinking in carbon composites, which identify the modes and morphology of kinking in fibrous materials, are presented. The thermodynamics and mechanics of kinking are analyzed. The analyses indicate the important role of matrix deformation (plastic and elastic) in determining the kink morphology, and identify the matrix yield strength and the distribution of fiber fracture strengths as the primary properties governing kink formation.

1.0 INTRODUCTION

It has recently been established that kinking is an important mode of structural degradation in fiber composites.[1-4] The first kinking observations were reported by Berg and Salama[1] for graphite/epoxy systems under axial compression, while more extensive studies of a similar system have subsequently been presented by Weaver and Williams.[2] These studies concluded that kinking was a direct consequence of microbuckling and invoked kink initiation concepts based on the critical stress for beam buckling on an elastic foundation.[5] The kink morphology was noted to be analogous to that observed in many other systems; notably, a kink inclination α equal to about twice the kink boundary orientation β, with β ranging between 20 and 30°. However, Argon[3] has noted that buckling usually occurs at much lower stresses than implied by the buckling equations, and attributes the disparity to the presence of inhomogeneities or prior fiber curvature. The evident extension of Argon's concept is the realization that kink formation is inhomogeneous and related to phenomena occurring during post-buckling deformation. More recently Chaplin[3] studied kinking in a glass fiber/epoxy system under axial compression. He confirmed the important role of microstructural inhomogeneities in kink formation, and noted that the simple relation between α and β coincides with a condition of zero volumetric strain in the kinked zone, suggesting a kink morphology determined in part by a maximum strain energy release rate criterion. However, he did not attempt a kinking analysis, and advanced no rationale for the importance of a zero volumetric strain (rather than zero shear strain) on the kink morphology.

A more detailed analysis of the kinking process is presented in this paper that correlates some of the key microstructural parameters that dictate

kinking, under conditions of both axial compression and of applied shear. The concepts and observations introduced by previous investigators are used where appropriate; while the additional experimental observations and measurements of kinking, required for the analytic developments, utilize information obtained on three-dimensional carbon/carbon composites (such as those used for re-entry vehicle nosetips) subjected to particle impacts.

Firstly, observations of kinking that establish the various modes of kink formation and provide a basis for kink analysis are presented, and micromechanical tests that evaluate the important mechanical properties of the composite constituents are described. Then, the thermodynamics and mechanics of kinking are explored to relate kink formation to the properties of the matrix and fibers and to the distribution of inhomogeneities.

2.0 EXPERIMENTAL

2.1 Materials and Test Methods

The materials employed in this study are three-dimensional carbon/carbon composites[6] that consist of carbon fibers with radius c, assembled in bundles of rectangular cross section, d_b, set in a graphite matrix[‡]. The bundles are oriented in three orthogonal directions, with the matrix filling the interstices between the bundles and the regions between individual fibers. A section that illustrates this geometry is presented in Fig. 1. Note that the matrix is a porous medium and that there are many pre-existing bundle fractures.

Samples of this material were subjected to localized impacts, either by 1 mm diameter glass spheres at velocities up to 6,000 ms^{-1} or by an instrumented 4 mm diameter steel sphere in a drop weight apparatus[7,8]. The samples were vacuum impregnated with polymer after impact and then sectioned to the impact site. The sections were mechanically polished prior to observing the damage in an optical microscope.

[‡]Most work was conducted on GE223, a material containing bundles ~400μm in width.

2.2 Kink Observations

Three principal modes of kinking have been detected in studies on carbon/carbon composites: kinking due to longitudinal compression (Fig. 2), lateral compression (Fig. 3), and lateral displacement or "shear" (Fig. 4). The kink morphologies for longitudinal compression and lateral displacement are very similar. The kink boundaries are approximately parallel and the fibers exhibit little residual curvature (Fig. 5a, b). The kinks can be either in-plane or out-of-plane on a specified section (Figs. 6, 2a, b). The in-plane kink and boundary orientation are relatively well-defined for broad kinks (ratios of kink width to bundle diameter $\gtrsim 0.1$), such that the kink orientation α ranges between 45° and 60° and the boundary orientation β is $\sim\alpha/2$, as shown by the experimented data summarised in Fig. 7. For narrower kinks, β increases and becomes more variable, while α tends to complete randomness. The fibers at the boundary are fractured (Fig. 8a, b), sometimes at several locations (Fig. 8b), but matrix fracture at the boundary is quite infrequent (Fig. 8a). Substantial voids are commonly observed where the kink boundary intersects the matrix (Fig. 8c). Arrested kinks are sometimes detected, the arrest being a direct consequence of either an interaction with a pre-existing defect (Fig. 2a) or with a prior kink (Fig. 2b). Partially formed kinks can also be detected (Figs. 4 and 9a, b). These provide invaluable information about the sequence of kink formation. In particular, it is apparent from Figs. 4 and 9b that kinks initiate from the "compressive" side of the distorted fiber bundle, while Figs. 9a, b indicate that the propagation of adjacent kink boundaries is not normally cooperative; rather, kink boundary propagation can be substantially independent. Kinking persists to very high temperatures (>3500° C) when the fibers exhibit some plasticity (Fig. 10). The kinks display more variable orientation relationships, and they generally arrest within bundles. The incidence of fracture at the boundary is also substantially reduced.

The kinking that results from lateral compression is more complex. There are no well-defined orientation relationships for the kinks, although the kink ends usually coincide with a lateral fiber bundle (Fig. 3a). The kinks are narrow and the fibers within the kink exhibit a multiplicity of orientations (Fig. 3b). Frequently, the matching fibers on opposite sides of the kink are subject to a substantial lateral displacement.

2.3 Micromechanics Tests

The elastic or plastic deformation of each constituent of a composite microstructure are two important properties affecting kink formation. The deformation characteristics can be estimated using microcompressive tests (Fig. 11a). The first test entails indenting each microcompressive zone (matrix, lateral fiber bundle, longitudinal fiber bundle) with a 400 μm diameter tungsten carbide hemisphere, and measuring the force (P), displacement (δ) characteristics. For elastic indentation the compliance (δ/P) affords a measure of Young's modulus E, through the relation;[8]

$$E = \left(\frac{P}{\delta}\right) \frac{(1-\nu^2)}{2a_r} \qquad (1)$$

where a_r is the radius of the hemisphere and ν is Poisson's ratio. Compliance relations obtained for each microstructural constituent are presented in Fig. 12a; the corresponding moduli obtained from the linear region are indicated on the figure. The lateral bundle modulus and the matrix modulus are found to be quite similar; this similarity is not surprising, since the lateral bundle modulus is dictated primarily by the continuous matrix phase. The longitudinal bundle modulus is over an order of magnitude larger, and consistent with the value anticipated from the fiber content of the bundles. The other important feature of the results is the onset of non-linearity in the matrix. This indicates the commencement of permanent deformation, probably due

to plastic deformation around the voids. The "effective" modulus of the matrix at large deformations is thus substantially smaller than the lateral modulus of the bundles. The deformation stresses cannot be determined from the elastic relations and a second test must be used. An appropriate test is a standard spherical indentation test, wherein the indentation pressure, p_i, can be related to the flow stress, σ_y, by a proportionality factor, $p_i \approx 3\sigma_y$. The results for the matrix and lateral deformation of the bundles indicate that $\sigma_y \sim 30$ MPa.

3.0 THERMODYNAMIC ANALYSIS

The morphology of kinking can be accounted for by examining the thermodynamic aspects of the kink propagation process (in a manner somewhat analogous to that utilized by Griffith[10] in his description of crack propagation). Additionally, some conception of the important considerations involved in kink interaction can be elucidated. Consider, for convenience, the kink depicted in Fig. 13a, under the action of a quasi-static applied shear stress τ_A. The resistance of the composite to deflection is supplied primarily by the relatively stiff carbon fibers (see Section 2.3) and the work performed by the applied stress is substantially compensated by an increase in strain energy in the fibers. However, this does not imply that the smaller increase in strain energy that occurs in the matrix can be neglected for purposes of kink analysis.

When the kink is initiated, several modes of energy redistribution occur. For fixed grip conditions (i.e., no work done by the applied shear stress), fiber fracture culminates in a decrease in fiber strain energy, ΔU_f, and a smaller increase in matrix strain energy, ΔU_m, (this is manifested as a decrease in the externally applied load), there is an increase in surface energy ΔS_f associated

with the fiber fracture surfaces, and plastic work ΔW_p is expanded in the matrix (see Section 2.3) to accommodate rotation of the fiber in the kinked zone.* The First Law energy balance during kinking is thus;

$$\Delta U_f = \Delta U_m + \Delta S_f + \Delta W_p \qquad (2)$$

Ideally, the energy balance should be conducted during a specified stage of kink propagation, to yield a complete relation between the various parameters involved in the kink propagation process. However, because of the relatively extensive transition zone (fig. 12b), such an analysis is complex and beyond the scope of the present paper. Instead, therefore, the energy balance is conducted between the unkinked and fully-kinked condition. It will be demonstrated that this mode of analysis yields a rationale for the observed kink morphology, and provides an upper limit on the kink formation condition, thereby elucidating some aspects of the kinking process.

3.1 Kink Morphology

A good estimate of the kink morphology can be obtained by analyzing the energy changes that occur in the matrix within the kinked zone; because the fiber contributions (surface and strain energy) and the matrix contributions outside the kinked zone appear to be largely independent of the kink orientation. The constancy of the surface energy is apparent from Fig. 8, where it is noted that the average orientation of the plane of fiber fracture is orthogonal to the fiber axis (as commonly encountered in brittle flexural failure). The invariant fiber strain energy is based on the premise that fiber fracture relieves the fiber strain over a specific distance from the fracture plane,

*Possible energy changes due to photon and phonon release[11] are not explicitly considered, because they are relatively ill-defined.

regardless of orientation. However, interaction effects between adjacent fractures comprising the kink could lead to some orientation dependence, especially in narrow kinks. Such an effect undoubtedly accounts for kink orientation anomalies at relative kink widths $\lesssim 0.1$ (Fig. 7).

The issues involved in the analysis of kink morphology can be nicely summarized in two schematics (Fig. 13). The first issue (Fig. 13a) concerns the fiber rotation, which determines the kink inclination α. It is evident from the schematic that if the fibers are reasonably well bonded to the matrix, i.e. at AA', BB', CC' etc. (this seems to be the case for carbon composites when no debonding has been observed. see Fig. 8), then the matrix within the kink (region AA' BB') must be subjected to a shear strain, ϕ. The relatively large magnitude of this strain indicates that it is primarily plastic* and constitutes an expenditure of plastic work. Also, unless matrix fracture occurs, two small zones near the kink boundaries, A'B'C and ABO, must undergo intense localized plastic deformation. This will inevitably lead to some void formation and "residual" elastic strain. However, we shall initially assume that the general plastic strain, ϕ, is the primary source of energy redistribution during fiber rotation and that the preferred fiber rotation is that which minimizes the expenditure of plastic work.

The second important feature of the kink morphology is the boundary inclination (Fig. 13b). It is apparent from the schematic that the major effect of changing the boundary orientation is to vary the state of normal strain in the matrix. Specifically, a small boundary inclination produces matrix compression, and a large boundary inclination generates matrix extension. An intermediate boundary orientation that minimizes the normal strain is thus

*A portion of the shear strain will, of course, be elastic (yielding an increase in elastic strain energy), but the observed kink orientations cannot be explained by assuming that the strain is fully elastic.

likely to exist. The plastic deformation of the matrix that occurs during fiber rotation (which, as noted above, dictates the kink orientation) should not lead to a significant volume change in the kinked zone (because volume is conserved during plastic deformation). Any volume change that is constrained to occur by prescribing the kink boundary orientation will thus be manifested as an increase in matrix strain energy. Hence, the optimum boundary orientation is initially assumed to be that which minimizes the volumetric elastic strain energy generated in the matrix, i.e. maximizes the strain energy release as in conventional fracture processes. A more exact solution would also take into account the "residual" elastic strain generated by fiber rotation and then minimize the total increase in strain energy.

3.1.1. Plastic Work

The plastic work expended during fiber rotation can be determined from the force on the fiber and the extent of fiber rotation. The force, dF, on an element, $d\ell$, of fiber located at a distance, ℓ, from the kink center (Fig. 12c) is related to the deformation pressure, p, by:

$$dF = 2cp\, d\ell \qquad (3)$$

For a small element of rotation $d\alpha$ (Fig. 12c) the work done against the matrix, dW, becomes:

$$dW = \ell dF d\alpha = 2cp\ell d\ell d\alpha \ . \tag{4}$$

The total work done, ΔW, for a rotation α_k is thus;

$$\Delta W = 4c \int_0^{\ell_k/2} \int_{\alpha_o}^{\alpha_k} p\ell d\ell d\alpha \ , \tag{5}$$

where ℓ_k is the kink length and α_o is the initial rotation at the kink zone (Appendix I). Since the pressure for a specified rotation is expected to be independent of the kink length, eqn. (5) reduces to:

$$\Delta W = \frac{c\ell_k^2}{2} \int_{\alpha_o}^{\alpha_k} p d\alpha \ . \tag{6}$$

However, the deformation pressure depends on the rotation through both the multiaxial yield criterion and the work hardening (Section 2.3). An analysis that includes both of these effects is a complex three-dimensional problem and is beyond the scope of the present paper. However, lower and upper bounds on the work done can be obtained by assuming, respectively, a constant pressure condition and a two-dimensional slip line field solution. For a constant pressure equal to the matrix yield stress, σ_{ym},

$$\Delta W = \frac{c\ell_k^2}{2} \sigma_{ym} (\alpha_k - \alpha_o) \tag{7}$$

For fixed grip conditions the kink width, w_d (Fig. 12a), is specified so that ℓ_k and α_k are related by:*

$$\ell_k = w_d \ \text{cosec} \ \alpha_k \ . \tag{8}$$

---

*This is a key aspect of the analysis, because a constant kink width requires the kink length to increase as the boundary inclination decreases. This increased volume of matrix subjected to deformation counteracts the reduced plastic work per unit length to yield the minimum.

Substituting ℓ_k from Eqn. (8) and α_o from Eqn. (A11) into Eqn. (7), the work done becomes;

$$\Delta W = cw_d^2 \sigma_{ym} \text{cosec}^2 \alpha_k \{\alpha_k - 2\tau_A (d_f+2c)^2 (d_b+d_s)^2 (3d_s^2 - 4w_d^2 \text{ cosec}^2 \alpha_R)/6\pi E_f c^4 d_b^2\} \quad (9)$$

where E_f is the fiber modulus, d_f is the fiber separation and d_s is the bundle separation. The preferred kink orientation, α_k^P, is obtained by differentiating Eqn. (9) with respect to α_k and setting the differential to zero. For $\alpha_R >> \alpha_o$, this yields;

$$\tan \alpha_k^P = 2\alpha_k^P \quad (10)$$

or,

$$\alpha_k^P = 67°$$

The corresponding minimum work, ΔW_{min}, is;

$$\Delta W_{min} = 0.7 \ \sigma_{ym} cw_d^2 \quad (11)$$

For larger α_o, α_k^P is a complex function of d_s/c, w_d/c, d_f/c and τ_A/E_f, ranging between ~ 60° and 67°. This range of α_k^P is close to the upper bound of the measured values (Fig. 7).

A two-dimensional slip line field solution[11] that closely resembles the deformation expected from fiber rotation is depicted in Fig. 15. The corresponding orientation dependencies of the normalized deformation pressures, $p/2k^*$, are plotted in Fig. 15 for two typical values of ℓ_k/d_b. Inserting p from Fig. 15 into Eqn. (6), and performing the integral numerically, yields α_K^P values of ~ 48°(ℓ_k/d_b = 0.3) and ~ 55° (ℓ_k/d_b = 0.5). These are within the range of the measured kink orientations. Detailed three-dimensional analyses should be capable of yielding more precise predictions of the kink orientation.

*k would be $\sigma_y/2$ for the Tresca criterion (σ_y is the uniaxial yield stress) and $\sigma_y/\sqrt{3}$ for the Von Mises criterion.

3.1.2 Strain Energy

The volumetric strain, ε_v, in the kinked zone consists of a uniaxial strain, ε_x, normal to the kink boundary, and is given by;[3]

$$\varepsilon_v \equiv \varepsilon_x = [\cos(\beta - \alpha_k)/\cos\alpha_k - 1]. \tag{12}$$

Hence, for a negligible "residual" elastic shear strain, the strain energy per unit volume, U, is simply;

$$U = \frac{E_m}{2} [\cos(\beta - \alpha_k)/\cos\ \alpha_k - 1]^2 , \tag{13}$$

and the strain energy in the kinked zone per unit thickness, U_k, is;

$$U_k = \frac{E_m}{2} \ell_k d_b \frac{\cos(\beta - \alpha_k)}{\cos\ \alpha_k} [\cos(\beta - \alpha_k)/\cos\ \alpha_k - 1]^2 . \tag{14}$$

where E_m is the matrix modulus and d_b is the bundle diameter. In the geometrically required angular range, $0 \leq \beta - \alpha_k \leq \pi/2$, Eqn. (14) shows that U_k exhibits only one minimum (equal to zero): at $\beta = 2\alpha_k^P$. This result is in reasonable accord with the experimental observations for broad kinks (Fig. 7), which indicate that β is slightly less than $2\ \alpha_k^P$. The small discrepancy is undoubtedly associated with the neglect of the "residual" strain energy; which would tend to produce a small matrix compression in order to accommodate the increase in matrix volume near the kink boundary (Fig. 13a).

3.2 Kink Formation

A thermodynamic analysis of kink formation would require, in addition to the analyses described above, at least an assessment of the strain energy changes that occur outside the kink zone, and of the surface energy created by fiber fracture (Eqn. 2). However, a preliminary estimate of the energy redistribution, suitable for qualitative identification of the important kink formation parameters, can be obtained by assuming that the strain energy in the fibers reduce to zero after kink formation. Then, the strain energy release per bundle, ΔU_b (Eqn. A6), is:

$$\Delta U_b = -\frac{9\tau_A^2}{2\pi^2 E_f d_b^2 c^2}(1+\nu)^2\,(d_f+2c)^2(d_b+d_s)^4\,d_s\left[0.37+\frac{0.01}{(1+\nu)^2}\left(\frac{d_s}{c}\right)^2\right]$$

The equivalent surface energy increase per bundle, ΔS_b, caused by fiber fracture is simply;

$$\Delta S_b = \frac{2\pi\gamma_f d_b^2 c^2}{(d_f+2c)^2}\,, \tag{15}$$

where γ_f is the "surface energy" of the fibers. Recalling that the matrix strain energy in the kinked zone is zero and neglecting the small strain energy increase in the matrix outside the kink, the strain energy release can be equated to the increase in fiber surface energy and matrix plastic work to obtain an approximate upper bound for the kink initiation stress, τ_k. Noting that the kink displacement term, w_d, in the plastic work expression can be equated* to the elastic displacement $2v_\ell$ (Appendix I) to obtain;

$$\Delta W_{min} = \frac{5}{\pi^2}\,\sigma_y\left(\frac{\tau_A}{E}\right)^2\frac{d_s^6\,(d_f+2_c)^4(d_b+d_s)^4}{c^7 d_b^4}\,, \tag{16}$$

the kink initiation stress becomes;

$$\tau_k^2 = \left(\frac{2\pi^3 E_f \gamma_f}{c}\right)\left[\frac{1}{(2+d_f/c)^4\,(1+d_s/d_b)^4\,(d_s/c)}\right] \tag{17}$$

$$\left\{\frac{1}{1.7(1+\nu)^2+0.05(d_s/c)^2-0.5(\sigma_{ym}/E_f)(d_s/c)^5\,[(d_f+2c)/d_b]^2}\right\}$$

*Applying the same approximation used to obtain the strain energy release, notably that the fiber strain after kinking is zero.

A plot (Fig. 15) of the normalized kink strength, $\tau_k^2 c/2\pi^3 \gamma_f E_f$, illustrates several important implications for kink formation; notably the strong retardation of kinking achieved by reducing d_s/c or d_s/d_b, and the potential for eliminating kinking by an appropriate enhancement of σ_{ym}/E_f. Also, the normalization indicates the direct importance of the fiber fracture energy, and modulus. More detailed implications are not warranted due to the approximate character of the analysis.

4.0 MECHANICS OF KINKING

Kink initiation cannot yet be adequately treated using a thermodynamic analysis (as noted above), but some additional insights can be gained by analyzing the stresses generated in the fibers. The "shear" kink is the most amenable to analysis and will be examined first.

4.1 "Shear" Kinks

The fiber stresses generated by a shear displacement are summarized in Appendix I. Fiber fracture will occur when the axial tensile stress exceeds the longitudinal strength S^* of a flaw located in the tensile zone. These flaws are statistically distributed in space and size, so that the fracture condition is probablistic in character (although fracture is most likely to occur near the zone of peak tensile stress). Techniques for deducing this fiber fracture condition will firstly be considered, and subsequently, the question of whether such fractures are a sufficient condition for kink initiation will be explored.

The flaw strength distribution required for fracture analysis can be determined by examining fiber fractures in regions where kink formation has not occurred (Fig. 16). If it is assumed that the matrix has a negligible effect on the stress in the fiber, the tensile stress σ_R at the (surface) fracture

*The strength of a flaw is the normal tensile stress required for the unstable propagation of that flaw to fracture.

site can be evaluated from the radius of curvature R, using;[13]

$$\sigma_R = \frac{E_f c \, \mathrm{Sin}\theta}{R} \tag{18}$$

where θ is the angular coordinate of the surface site relative to the position of peak tensile stress. Then, equal length regions with that curvature can be randomly sampled to determine the proportion of fractures. This proportion is a direct measure of the fracture probability, $\Phi(S)$. Continuing in this fashion, by sampling regions of different curvature (but all of the same length, ℓ_R), a fracture probability, strength curve can be developed (Fig. 17a). The flaw density function $g(S)dS$[14,15] (the number of flaws per limit volume, or area, with a strength between S and S + dS) can now be derived. If the reasonable assumption is made that fracture is surface flaw initiated, g(S) is given (eqn. (A16)) by;

$$g(S) \approx \frac{1}{\pi c \ell_R} [2\xi' + S\,\xi'']$$

where $\xi = -\ell n[1 - \Phi(S)]$. The flaw density curve derived from Fig. 17a using eqn. (A16) is plotted in Fig. 17b. The resultant probabilities of first fracture in a "sheared" fiber bundle can be derived from Fig. 17b as described in Appendix II.

It seems unlikely that the onset of first fracture necessarily coincides with kink initiation, because fractures are frequently observed in regions remote from kink boundaries (Fig. 16). A more likely condition for kink formation is the creation of several fiber fractures in the outermost layers of the bundle. These fibers are not fully constrained, and

they can rotate in a sense that substantially enhances the stress in the next layer of fibers (Fig. 18), thereby initiating the sequence of fractures that constitute a kink. Should this kink formation mechanism pertain, the kink formation stress can be deduced by estimating the probability that an unstable fracture occurs in the outer layer. The factors that influence this probability can be estimated from a two-dimensional model[3] that incorporates both the statistical character of fiber fracture and the stress enhancement imparted by the matrix phase.

The numerical details of the model have been established for the following strength distribution function;

$$\int_0^S g(S)dS = \lambda(S/S_o)^m \qquad (19)$$

where S_o, λ and m are constants. The present data for fiber fracture (Fig. 17b) are moderately well described by this relation, with m = 8. The key aspect of the analysis for present purposes concerns the instability condition, which is expressed in terms of both the number of fiber fractures and the fracture stress. The analysis obtains fracture expressions for either elastic or plastic matrix deformation within the zone of stress enhancement (Fig. 19). We shall assume that, for kink initiation purposes, the matrix behaves plastically (see sections 2, 3). Then a stress enhancement factor κ_n, which is a measure of the increased probability of failure in a zone adjacent to n fractured fibers (Fig. 19), can be defined as[3];

$$\kappa_n \approx \left\{1 + \frac{\sigma_{ym}}{\pi\sigma}\,\omega^{1/2}\,\ln\left[\frac{n}{\omega}\left(\frac{\pi\sigma}{\sigma_{ym}}\right)^2\right]\right\} f(m) \qquad (20)$$

where

$$\omega = \frac{E_f}{\mu_m} V_f (1-V_f)$$

V_f is the volume fraction of fibers, σ is the "remote" stress and $f(m)$ is a slowly varying function, equal to 0.88 for m = 8.

The probability of crack extension $\Phi(\sigma)$ at the stress σ for a crack consisting of n broken fibers is

$$\Phi(\sigma) = NA_o A_1^2 A_3^2 \ldots A_n^2 (1 - A_o)^{N-n} \qquad (21)$$

where

$$A_o = 1 - \exp(-S^*)$$
$$A_n = \exp(-S^*) - \exp(-\kappa_n^m S^*)$$

and N is the number of fibers in the bundle. The condition for unstable extension of the crack is;

$$\kappa_n^m (S/S_o)^m w \delta \lambda \equiv \kappa_n^m S^* = \ell n [1/(1 - \Phi_o)] \qquad (22)$$

where w is the laminate width, Φ_o is the associated probability level, and δ is the extent of the stress enhancement zone

$$\delta = \frac{\pi^2}{2} \left(\frac{\sigma}{\sigma_{ym}}\right)^2 \frac{cn}{\omega^{1/2}} \qquad (23)$$

Equating the stress to the fiber strength S, eqns. (19 to 23) can be solved

numerically for the number of fiber fractures at instability, N_c. The quantity N_c is relatively insensitive to the material parameters. For values of the material parameters typical of carbon composites (see section 2.3, 4.1), m = 6 to 10, $\sigma_{ym}/S_o = 10^{-3}$ to 10^{-1}, E_f/μ_m = 10 to 100 and V_f = 0.7 to 0.9, setting the probability $\Phi(S)$ equal to 0.5 (its median value) and Φ_o equal to 0.99 (a high probability of instability) gives $N_c \sim 3$. It has been demonstrated for this value of N_c[3], that the critical "remote" stress for unstable crack growth, σ_c (equivalent, on the basis of the present premise, to the kink formation stress) can be derived explicitly for large N as;

$$\sigma_c = f(N,m)\ [w\,\delta\,\lambda\ (K_3^m - 1)/S_o^m]^{-1/m} \tag{24}$$

where f (N,m) is a weak function of N and m. Substituting for δ and K_3^m from eqns. (23) and (19) allows eqn. (24) to be expressed as;

$$\left(\frac{S_o}{\sigma_{ym}}\right)^m = \frac{3\pi^2}{2\omega^{1/2}}\left(\frac{\sigma_c}{\sigma_{ym}}\right)^{m-2} \lambda wc \left\{\left[1 + \frac{\omega^{1/2}}{\pi}\left(\frac{\sigma_{ym}}{\sigma_c}\right) \ell n\, \frac{3\pi^2}{\omega}\left(\frac{\sigma_c}{\sigma_{ym}}\right)^2\right]^m - 1\right\} \tag{25}$$

For small σ_y/σ_c this can be simplified to;

$$\frac{S_o}{\sigma_{ym}} = \left(\frac{\sigma_c}{\sigma_{ym}}\right)^{1-3/m}\left[\frac{3\pi m\lambda wc}{2}\ \ell n\, \frac{3\pi^2}{\omega}\left(\frac{\sigma_c}{\sigma_{ym}}\right)^2\right]^{1/m} \tag{26}$$

Inspection of eqn. (26) indicates that the critical stress depends primarily on the matrix yield strength σ_{ym} and the fiber fracture parameters S_o and m; the matrix modulus, fiber volume fraction (and the fiber dimensions) are secondary (but not negligable) considerations, except as σ_c/σ_y approaches unity.

Further, the matrix yield strength is only effective when m is small, $\lesssim 10$ (i.e. the variability in the fiber fracture strength is large), as illustrated in Fig. 20. These considerations could be used to design fiber composites with a maximum resistance to kink formation, primarily by increasing the fiber fracture strength level S_o and (except for low fiber strength variability) by enhancing the matrix yield strength. Additionally, for "shear" induced kinks, some further considerations emerge when σ_c is related to τ_A through eqns. (A1) and (A2), viz;

$$\tau_{A_c} = \frac{\pi c \sigma_c}{3 d_s} (2 + d_f/c)^2 \, (d_s/d_b + 1)^2 \qquad (27)$$

Hence, as might be intuitively expected, small relative fiber separations, d_f/c, and bundle separations, d_s/d_b, and large fiber diameters also enhance the "shear" kink resistance of the composite.

The preceding discussion of kinking has, for simplicity, emphasized kink formation under conditions of lateral displacement. However, in order to provide a more comprehensive overview of mechanical degradation, the kinking that occurs under longitudinal and lateral compression will also be briefly discussed.

4.2 Compressional Kinks

The kink morphology under longitudinal compression is identical to that observed for lateral displacement and can be accounted for using analogous thermodynamic concepts. But, the kink formation condition will differ because the fiber deformations (and hence the strain energy release and the tensile stress distribution) are substantially different. An upper bound on the kink initiation

condition will be the critical compressive stress, σ_{cr}, for the elastic buckling of a fiber or a bundle. However, as noted by Argon[3] and Chaplin[4], local inhomogeneities can cause compressive failures at substantially lower stresses. The inhomogeneities that could lead to premature buckling are exemplified by localized bundle curvature (Fig. 1), large matrix voids (Fig. 1) etc. The presence of these inhomogeneities would reduce the critical buckling stress to a modest level. A simplified model of buckling induced by a shear instability[3] indicated that the critical buckling stress, σ_{cr}, for a misaligned laminate is;

$$\sigma_{cr} \approx \frac{\sigma_{ym}}{2\theta_o} \tag{28}$$

where θ_o is the initial misalignment. The onset of buckling for this mode of instability would thus be primarily related to the matrix yield strength and the fiber misalignment. This former dependence is consistent with many compressive strength measurements on fiber composites.[17] Whether the onset of buckling is a sufficient condition for kink formation is determined by the character of the composite and by the imposed boundary conditions. If the buckling instability in the fiber bundle is constrained by the presence of a lateral surrounding medium (e.g. as in some carbon/carbon composites) or by a "fixed grip" type of boundary, the post-buckling elastic deformation of the fibers and the plastic deformation of the matrix would dictate kink initiation, in much the same sense as kink formation under lateral displacement. An analogous analysis of fiber fracture would then indicate the relative role of the fiber fracture strength and the matrix yield strength in kink formation. Conversely, if the buckling were unstable, then fiber bending would inevitably continue until the tensile stress in the fibers increased to the fracture strength and kinking would ensue. Kink formation would then be independent of the fiber properties.

Kinking under lateral compression is quite different in character from the two other modes. The kink morphology is not governed by simple thermodynamic concepts. Local stress concentrations probably dominate this mode of kinking. The kinking cannot be accounted for by a symmetric pressure between two opposing bundles (Fig. 21), because the dominant stress is a transverse compression[9] (Fig. 21) that cannot induce kink formation. However, if the opposing bundles are slightly displaced (Fig. 20), very large transverse shear stresses develop[9] (Fig. 21). These shear stresses are postulated to be the primary cause of lateral kinking. The situation is analogous to the kinking generated by lateral displacement, except that d_s is very small and kinking is constrained to occur in a narrow zone defined by the zone of action of the transverse shear. The kink formation and morphology is thus determined by the details of the pressure distribution imposed by the opposing fiber bundles and (to a lesser extent) by the matrix. This type of problem can be analyzed using Fourier series[9] and studies are in progress to obtain specific relations between pressure distributions and kink formation.

5. Implications and Conclusions

Observations of kinking in carbon composites have indicated that kinking can occur under longitudinal compression, lateral compression and lateral displacement. The kink morphologies are relatively well defined for broad kinks but become more random for narrow kinks.

A thermodynamic analysis of kinking has accounted for the observed kink morphologies in terms of the strain energy and plastic work associated with the matrix phase. Specifically, minimization of the plastic work dictates the kink inclination, while minimization of the elastic strain energy determines the kink boundary orientation. The analysis has also highlighted the important role

of the matrix yield strength and the fiber fracture resistance in kink formation, in the sense that kinking is retarded by large matrix yield strength and fiber fracture resistance .

The mechanics of kinking have then been explored using a model for statistical fiber fracture and matrix stress enhancement. The appropriate fracture and deformation parameters have been determined in-situ for the present carbon composite, and these parameters have been used to obtain an approximate expression for the critical kink formation stress. This expression confirms the central importance of large matrix yield strength on kink suppression, and indicates the varied role of the fiber fracture strength and variability.

The importance of fiber and bundle dimensions and separations on kink formation depends on the mode of kinking. But, in most instances, a large proportion of fibers oriented in a sense that minimizes fiber deflection is preferred, e.g. a small relative bundle separation, d_s/d_b.

APPENDIX I

ANALYSES OF BUNDLE DEFORMATION

1. Strain Energy

The stresses and displacements in a laterally displaced ligament (figure 22) can be deduced by noting that the ligament deformation is equivalent to that of two opposing rigidly mounted cantilevers in intimate contact.[9] The cantilever solution indicates that the stresses in each fiber are;[9]

$$\sigma_x = \frac{-6P\,xy}{\pi c^4} \quad ; \quad \sigma_y = 0$$

$$\tau_{xy} = \frac{-12P}{\pi c^2}\left[1 - \frac{y^2}{c^2}\right] \qquad \text{(A1)}$$

where P is the force acting on the fiber ends and the x and y axes are indicated on Fig. 22. For a symmetric three-dimensional fiber composite (Fig. 1) in which the deflection resistance is supplied primarily by the fibers, P is related to the applied shear stress τ_A, by;

$$P = \tau_A (d_f + 2c)^2 (d_b + d_s)^2/d_b^2 \qquad \text{(A2)}$$

where d_f is the separation between fibers, d_b the bundle diameter and d_s the separation between bundles.

The strain energy dU in a volume element, dxdrdθ is given by;

$$dU = \frac{c}{2E_f}\left[\sigma_x^2 + \sigma_y^2 + 2\tau_{xy}^2 \quad (1+\nu)\right] dxdrd\theta \tag{A3}$$

Expressing the stresses from eqns. (A1) and (A2) in cylindrical coordinates, and substituting into eqn. (A3), the total strain energy in each fiber U_f becomes;

$$U_f = \frac{9\tau_A^2(d_f+2c)^4}{2\pi^2 E_f c^3 d_b^4}(d_b+d_s)^4(1+\nu)^2 \int_0^{\pi/2}\int_0^{c}\int_0^{d_s/2}\left[1+4\frac{x^2r^2\cos^2\theta}{c^4(1+\nu)^2} - \frac{2r^2\cos^2\theta}{c^2} + \frac{r^4\cos^4\theta}{c^4}\right] dxdrd\theta \tag{A4}$$

Integration then gives,

$$U_f = \frac{9\tau_A^2}{2\pi^2 E_f d_b^4 c^2}(1+\nu)^2(d_b+d_s)^4(d_f+2c)^4 d_s\left[0.37 + \frac{0.01}{(1+\nu)^2}\left(\frac{d_s}{c}\right)^2\right] \tag{A5}$$

The total strain energy in the bundle, U_b, is thus;

$$U_b = \frac{9\tau_A^2}{2\pi^2 E_f d_b^2 c^2}(1+\nu)^2(d_f+2c)^2(d_b+d_s)^4 d_s\left[0.37 + \frac{0.01}{(1+\nu)^2}\left(\frac{d_s}{c}\right)^2\right] \tag{A6}$$

2. Initial Inclination

The displacement, v, of a fiber subjected to a shear force, P (Fig. 22) is[9],

$$v = \frac{2P}{3\pi c E_f}\left[2(d_s/c)^3 + 3(x/c)\left[\nu-(d_s/c)^2\right] + (x/c)^3\right] \qquad (A7)$$

The initial inclination α_o in the kinked zone is related to v by;

$$\sin\alpha_o = \frac{v_\ell - v}{\ell_k} \qquad (A8)$$

where v_ℓ is v at x = o. Substituting for v and v_ℓ, eqn.(A8) becomes,

$$\sin\alpha_o = \frac{2Px}{3\pi c^2 E_f \ell_k}\left[3(d_s/c)^2 - (x/c)^2 - 3\nu\right] \qquad (A9)$$

For small α_o ($\sin\alpha_o \approx \alpha_o$, $x \approx \ell_k$) and for a relatively broad kink ($d_s > \ell_k >> c$), eqn. (A9) reduces to;

$$\alpha_o = \frac{2P}{3\pi c^4 E_f}(3d_s^2 - \ell_k^2) \qquad (A10)$$

or, expressed in terms of the applied shear stress, τ_A,

$$\alpha_o = \frac{8\tau_A (d_f + 2c)^2}{3\pi E_f c^4 d_b^2}(3d_s^2 - \ell_k^2)(d_b + d_s)^2 \qquad (A11)$$

APPENDIX II

FRACTURE PROBABILITIES

1. Pure Bending

The probability of fracture at a stress S in a body of volume V for a flaw density g(S)dS is given by;[14,15]

$$\xi(S) = -\ell_n[1 - \Phi(S)] = -\int_V dV \int_o^S g(S)dS \qquad (A12)$$

For fibers subjected to pure bending, the surface tensile stress (see eqn. 8) is[13]

$$S = \frac{E_f c \sin\theta}{R} = S_m \sin\theta$$

where S_m is the peak tensile stress. Hence, for surface controlled fracture, the probability of fracture for a fiber of length ℓ_R and radius c is;

$$\xi(S_m) = -2c\ell_R \int_\theta^{\pi/2} d\theta \int_o^{S_m \sin\theta} g(S)dS \qquad (A13)$$

Changing the order of integration yields,

$$\xi(S_m) = 2\ell_R c \int_o^{S_m} \sin^{-1}(S/S_m)\, g(S)dS \qquad (A14)$$

It is not possible to obtain $g(S_m)$ for this distribution in the usual fashion without assuming a priori that it has a specific functional form.[14,15] A useful

working result can be obtained, however, if the following approximate stress is applied;

$$S = S_m\,(1 - 2\theta/\pi) \tag{A15}$$

Then $g(S_m)$ is given by;[15]

$$g(S_m) = \frac{1}{\pi c \ell_R}\,[2\xi'(S_m) + S_m\xi''(S_m)] \tag{A16}$$

2. Laterally Displaced Fiber Bundle

The tensile stress in a fiber subjected to a lateral displacement can be expressed (see eqn. A1) as;

$$S = S_m \sin\theta\,(1 - 2x/d_s) \tag{A17}$$

where $S_m = 3\tau_A\,(d_f + 2c)^2\,d_s/c^2$. Hence, the fracture probability becomes

$$\xi(\tau_A) = -4c \int_0^{d_s/2} dx \int_0^{\pi/2} d\theta \int_0^{S_m \sin\theta(1-2x/d_s)} g(S)\,dS \tag{A18}$$

Changing the order of intergration reduces eqn. (A18) to;

$$\xi(\tau_A) = -2cd_s \int_0^{S_m} \left[\sin^{-1}(S/S_m) - (S/2S_m)\,\ell n\,\frac{1 - \sqrt{1-(S/S_m)^2}}{1 + \sqrt{1-(S/S_m)^2}}\right] g(S)\,dS$$

$$\equiv -2cd_s\,\chi\,(\tau_A) \tag{A19}$$

The equivalent probability of first fracture in a fiber bundle, ξ_b is

$$\xi_b(\tau_A) = \frac{\xi(\tau_A) d_b^2}{(d_f + 2c)^2} \qquad \text{(A20)}$$

ACKNOWLEDGEMENTS

The authors wish to thank the Office of Naval Research for their financial sponsorship of the work described in this paper under contract N00014-76-C-0854.

REFERENCES

1. C. A. Berg and M. Salama, Fiber Sci. Tech. 6 (1973) 79.

2. C. W. Weaver and J. G. Williams, Jnl. Mater. Sci. 10 (1975) 1323.

3. A. S. Argon, Treatise on Materials Science and Technology (Academic Press, N.Y.), Vol. 1 (1972)p. 79.

4. C. R. Chaplin, Jnl. Mater. Sci. 12 (1977) 347.

5. H. Schuerch, AIAA Journal 4, Jan. 1966.

6. D. F. Adams, Mater. Sci. Eng. 23 (1976) 55.

7. M. E. Graham, J. D. Carlyle and T. L. Menna, Rev. Sci. Inst. 46 (1975) 1221.

8. J. A. Aleszaka, M. Ferdman, and W. F. Adler, Dynamic Properties of Carbonaceous Materials, Technical Report in Preparation for the Space and Missiles Systems Organization.

9. S. Timoshenko and J. N. Goodier, Theory of Elasticity, (MaGraw-Hill, N.Y.), 1950.

10. A. A. Griffith, Phil. Trans, Roy. Soc. A221 (1920) 163.

11. A. G. Evans and T. G. Langdon, Prog. Mater. Sci., 21 (1976) 171.

12. R. Hill, The Mathematical Theory of Plasticity (Clarendon Press, Oxford) 1956.

13. S. Timoshenko, Strength of Materials (Van Norstrand, N.Y.) 1955.

14. J. R. Matthews, F. A. McClintock and W. Shack, Jnl. Amer. Ceram. Soc. 59 (1976) 304.

15. A. G. Evans and R. L. Jones, Jnl. Amer. Ceram. Soc., in press.

16. S. Timoshenko and J. M. Gere, Theory of Elastic Stability (McGraw-Hill, N.Y.) 1961.

17. L. J. Broutman, Modern Composite Materials (Ed., L. J. Broutman and R. H. Krock), Addison-Wesley, Reading, MA (1967) p. 337.

FIGURE CAPTIONS

Fig. 1. A section through a carbon/carbon composites indicating the as-fabricated microstructural condition*; the section exposes lateral fiber bundles and highlights the presence of matrix voids, bundle fractures and local bundle curvature.

Fig. 2. Kinks generated by longitudinal compression (a) broad kinks showing in-plane and out-of-plane morphologies and kink arrest at a pre-existing void (b) broad kinks showing kink arrest at another kink boundary (c) intermediate kinks with small fiber rotation (d) an intermediate kink with a large fiber rotation (e) arrays of intermediate kinks indicating a range of orientations (f) narrow kinks indicating a typical kink orientation (g) a narrow kink indicating the large fiber rotation.

Fig. 3. Kinks generated by lateral compression (a) typical kink morphologies (b) the multiplicity of fiber orientations within the kink.

Fig. 4. Kinks formed by lateral displacement indicating typical kink morphologies.

Fig. 5. Kinks produced by lateral displacement indicating (a) the approximate parallelism of the bounderies (b) the lack of residual fiber curvature.

Fig. 6 A schematic indicating the morphology of in-plane and out-of-plane kinks.

Fig. 7. Kink orientation relationships as a function of relative kink width for kinks produced by longitudinal compression or lateral displacement.

Fig. 8. Kink boundaries indicating (a) the fracture of fibers and infrequent matrix fracture (b) single and multiple fiber fracture (c) a void at a bundle/matrix interface.

Fig. 9. Partially formed kinks (a) single boundary formation (b) double boundary.

---

*All micrographs in this paper are optical, taken in polarized reflected illumination.

Fig. 10. Kinking at elevated temperatures (3500°C)

Fig. 11. Compliance curves obtained for various microstructural constituents.

Fig. 12. (a) A schematic indicating the formation of a "shear" kink. (b) a schematic indicating the transition zone between the fully-kinked and unkinked zone. (c) the elements used to evaluate the plastic work expended against the matrix during fiber rotation.

Fig. 13. Two schematics illustrating the principles governing the kink morphology (a) the matrix shear and local distortion caused by fiber rotation (b) the matrix compression or extension and its relation to the kink boundary inclination.

Fig. 14. A slip line field for ironing of a thin-walled cylinder[11], and the deformation pressure as a function of orientation for two (fixed) values of the relative kink width, ℓ_k/d_b.

Fig. 15. A schematic indicating the matrix strain for large and small boundary inclination.

Fig. 16. Fiber fracture in regions of fiber curvature remote from kink boundaries.

Fig. 17. (a) A fracture probability, strength curve for fracture of the carbon fibers in the present composite. (b) The flaw density as a function of flaw strength derived from (a).

Fig. 18. A schematic indicating the stress transmission through the matrix caused by an outer fiber fracture that could induce the kink instability.

Fig. 19. A schematic indicating the basis for a bundle fracture model involving fiber fracture enhancement through matrix stress transmission.

Fig. 20. A plot of the normalized kink formation stress σ_c/σ_{ym} as a function of the inverse of the normalized fiber fracture strength, S_o/σ_{ym}, for several values of the strength distribution term, m.

Fig. 21. The stresses that develop in a beam compressed between two opposing, displaced pressure zones.

Fig. 22. A cantilevered beam and the dimensions used to calculate the stresses, displacements and strain energy in "sheared" fiber bundles.

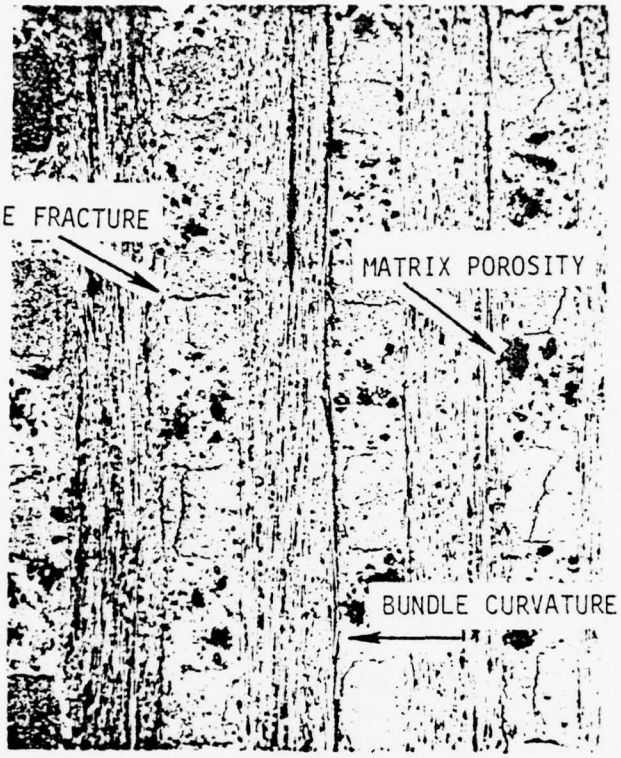

Figure 1

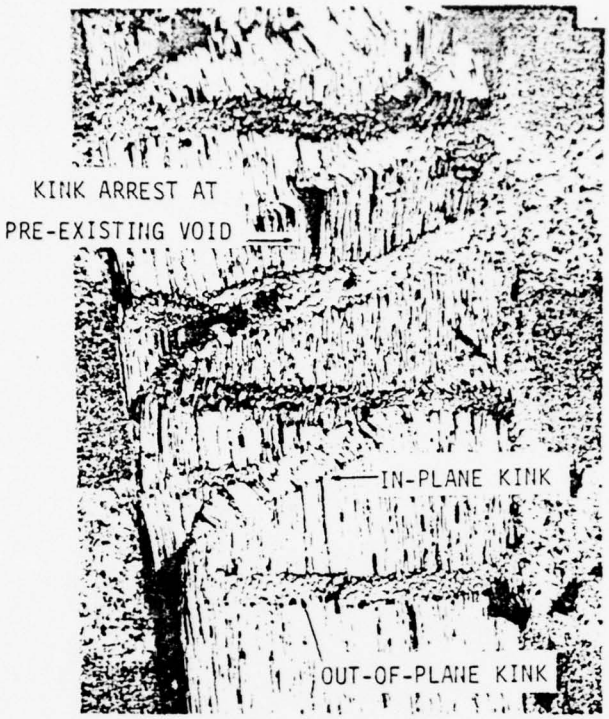
KINK ARREST AT
PRE-EXISTING VOID
IN-PLANE KINK
OUT-OF-PLANE KINK


b
KINK ARREST AT
KINK INTERSECTION

Figure 2

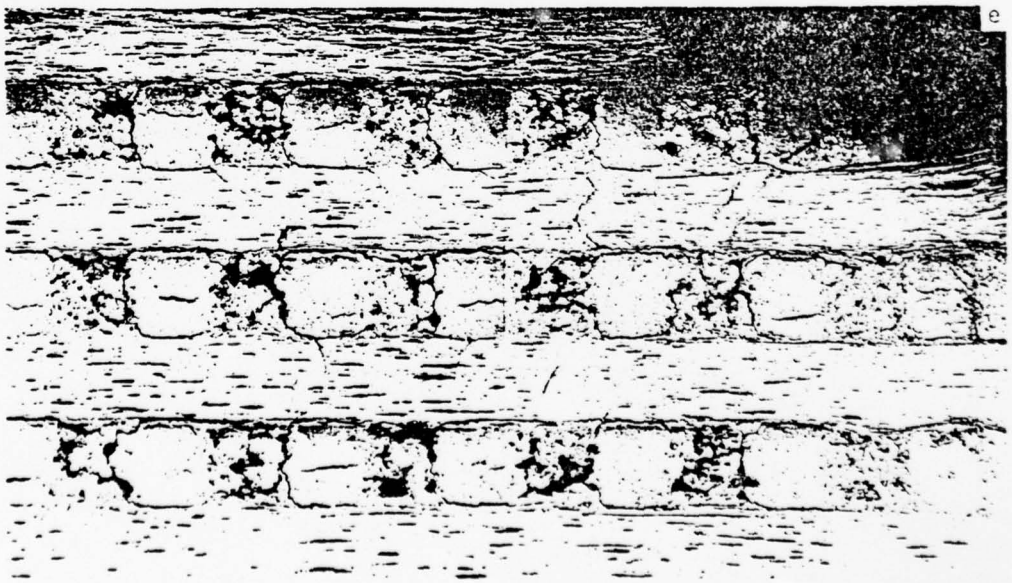

Figure 2

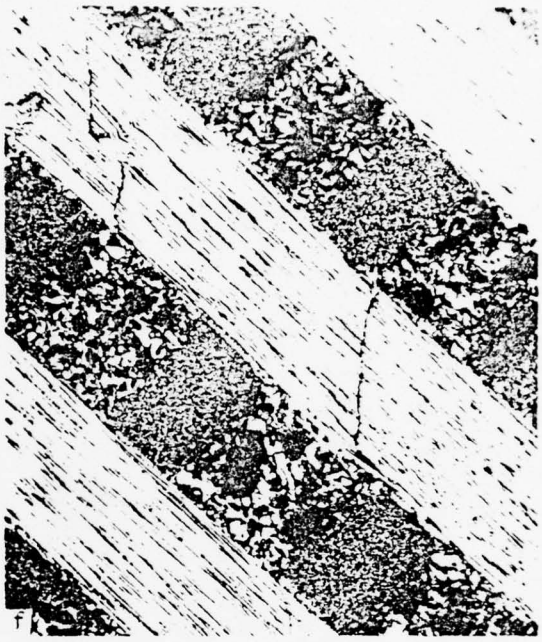

Figure 2

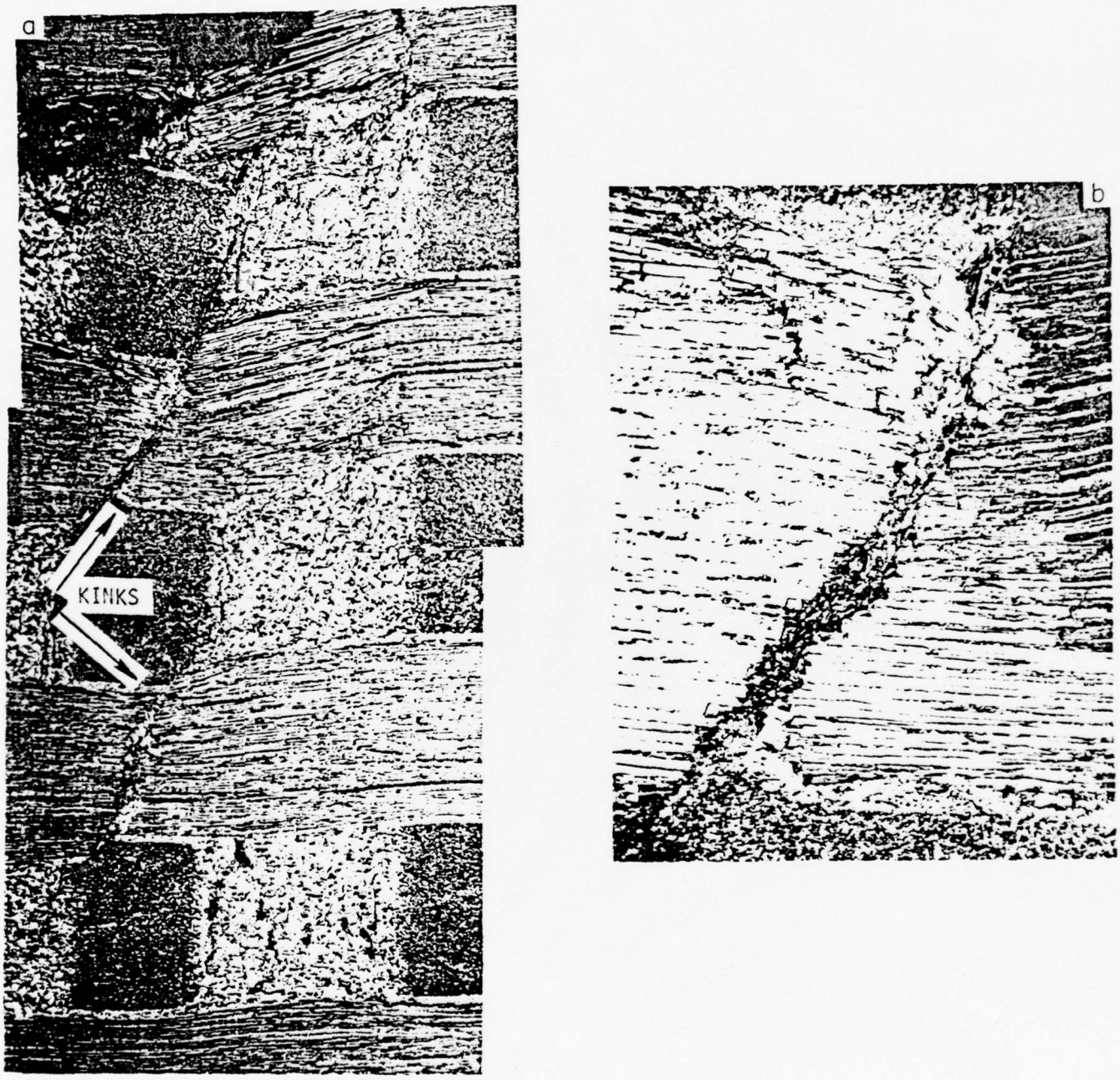

Figure 3

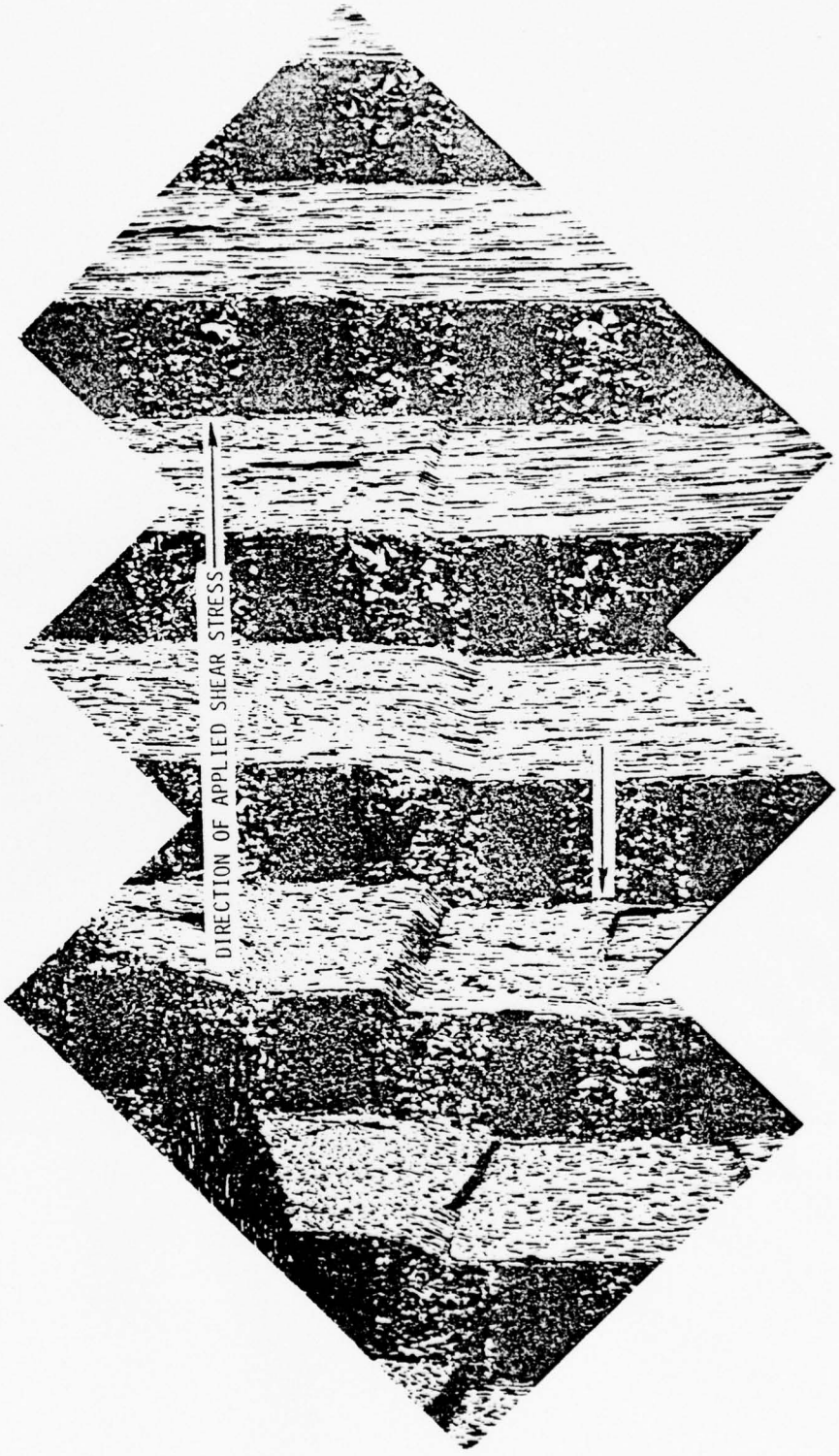

Figure 4

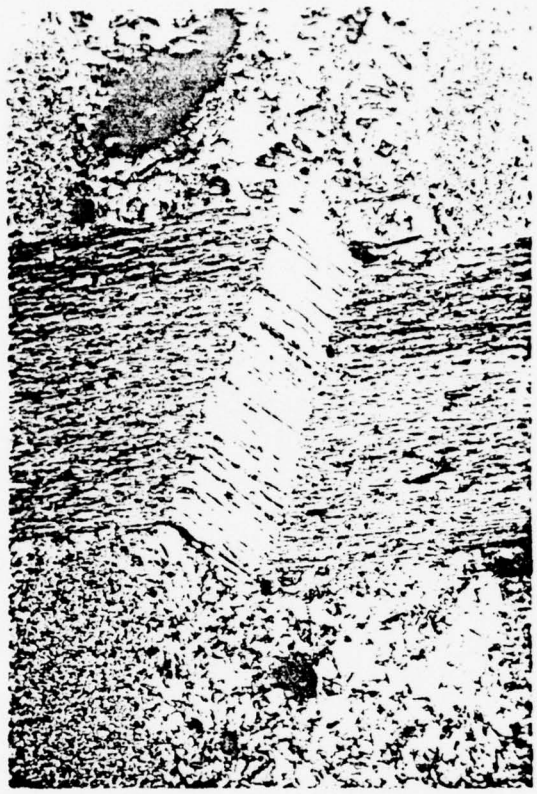

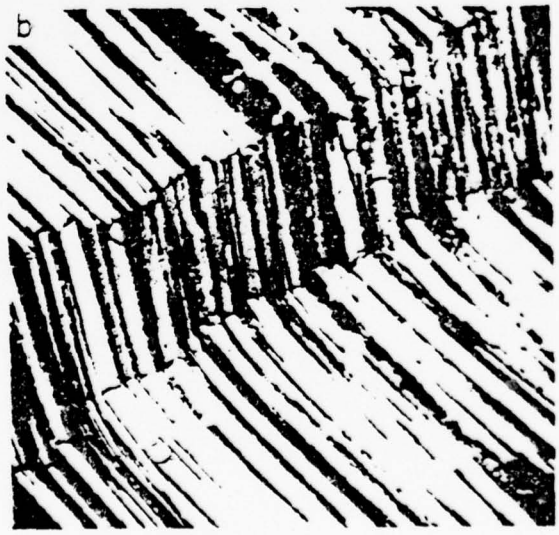

Figure 5

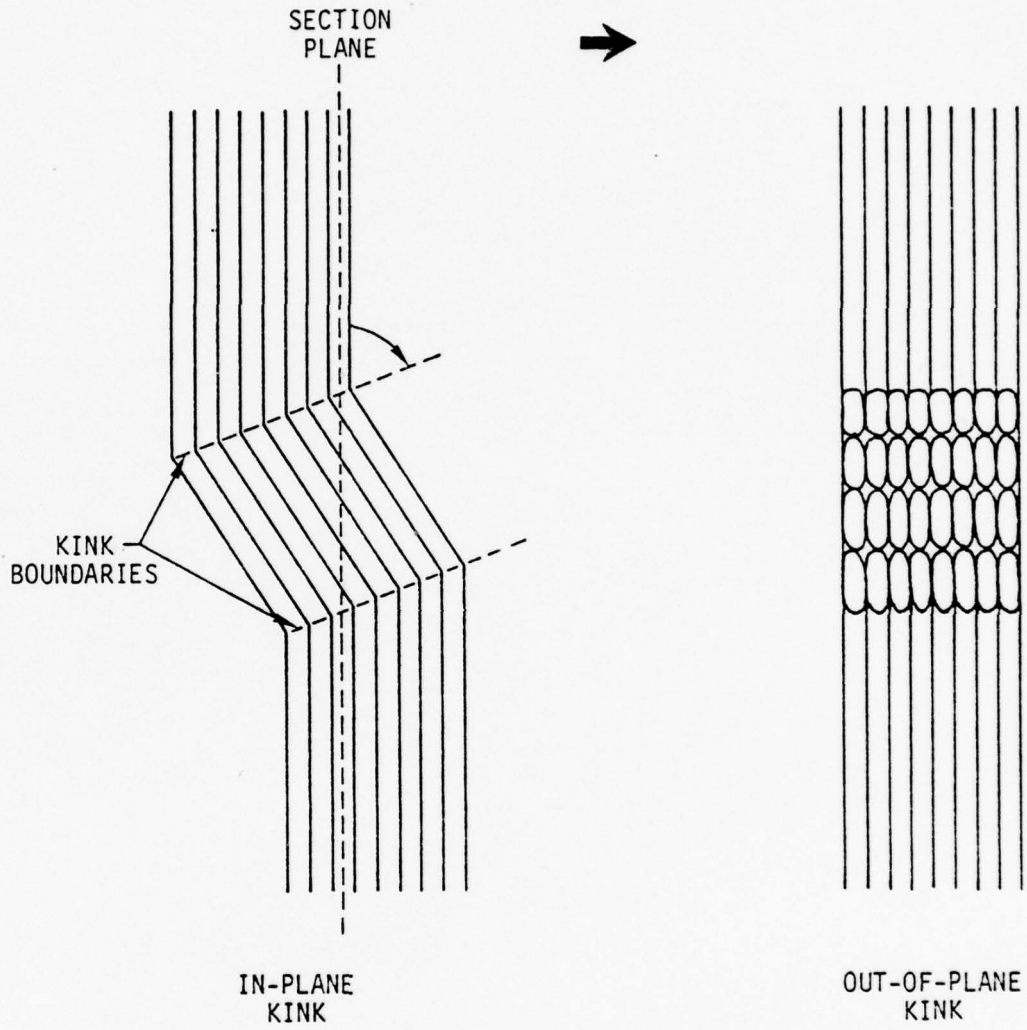
SECTION
PLANE
KINK
BOUNDARIES
IN-PLANE
KINK
OUT-OF-PLANE
KINK

Figure 6

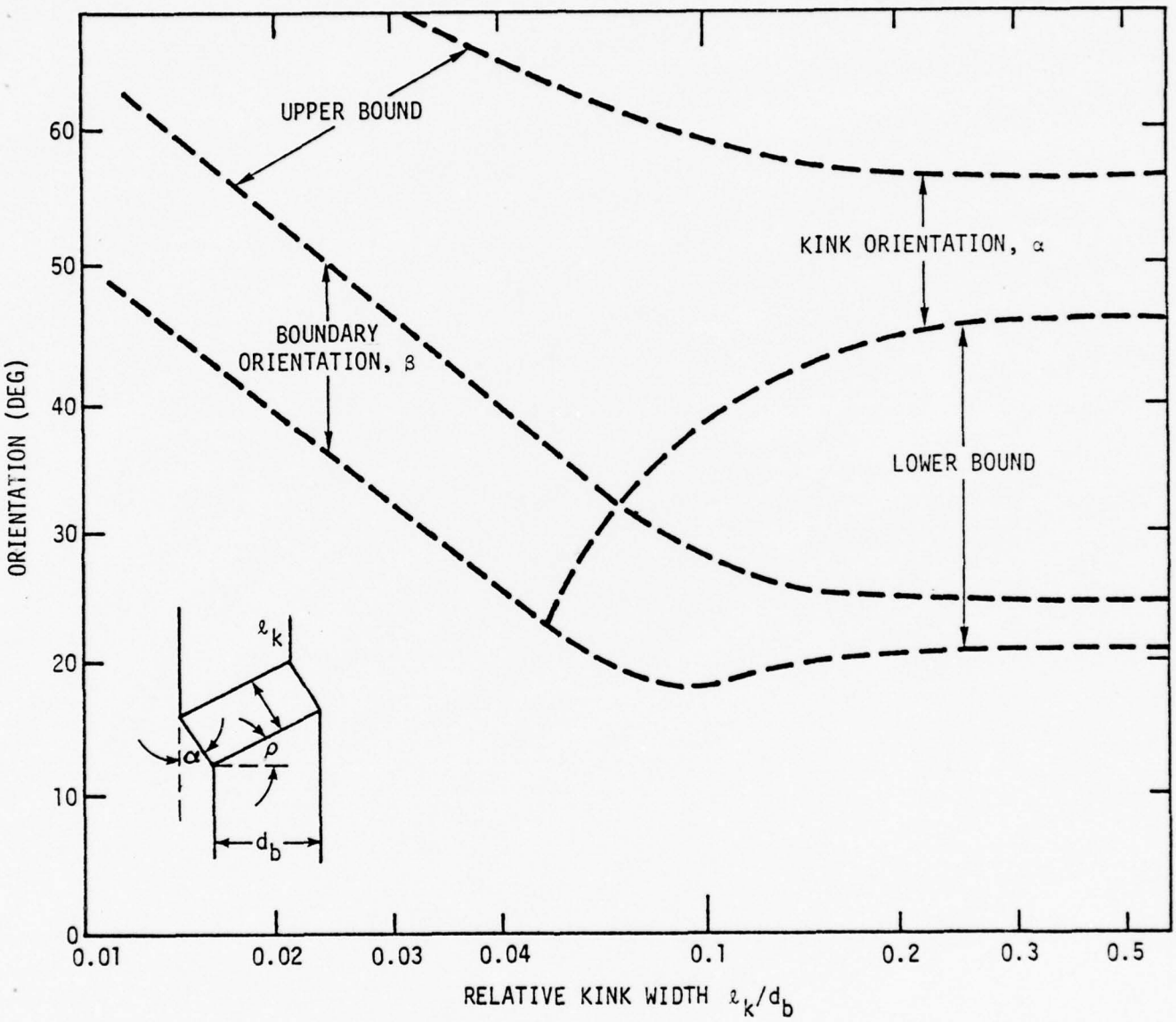
UPPER BOUND
KINK ORIENTATION, α
BOUNDARY ORIENTATION, β
LOWER BOUND
ORIENTATION (DEG)
RELATIVE KINK WIDTH ℓ_k/d_b
ℓ_k
α
ρ
d_b
0
10
20
30
40
50
60
0.01
0.02
0.03
0.04
0.1
0.2
0.3
0.5

Figure 7

Figure 8

Figure 9

Figure 9

Figure 10

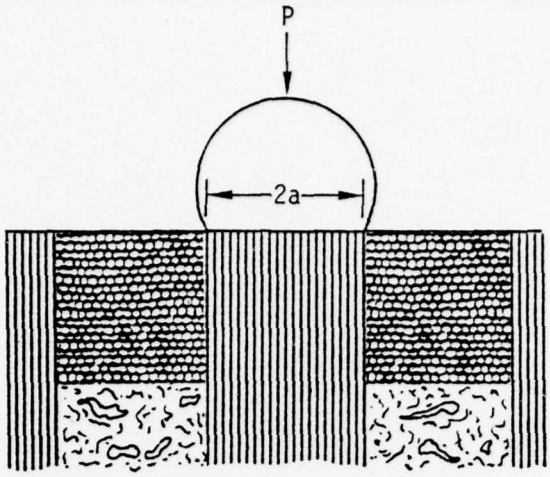
P
2a

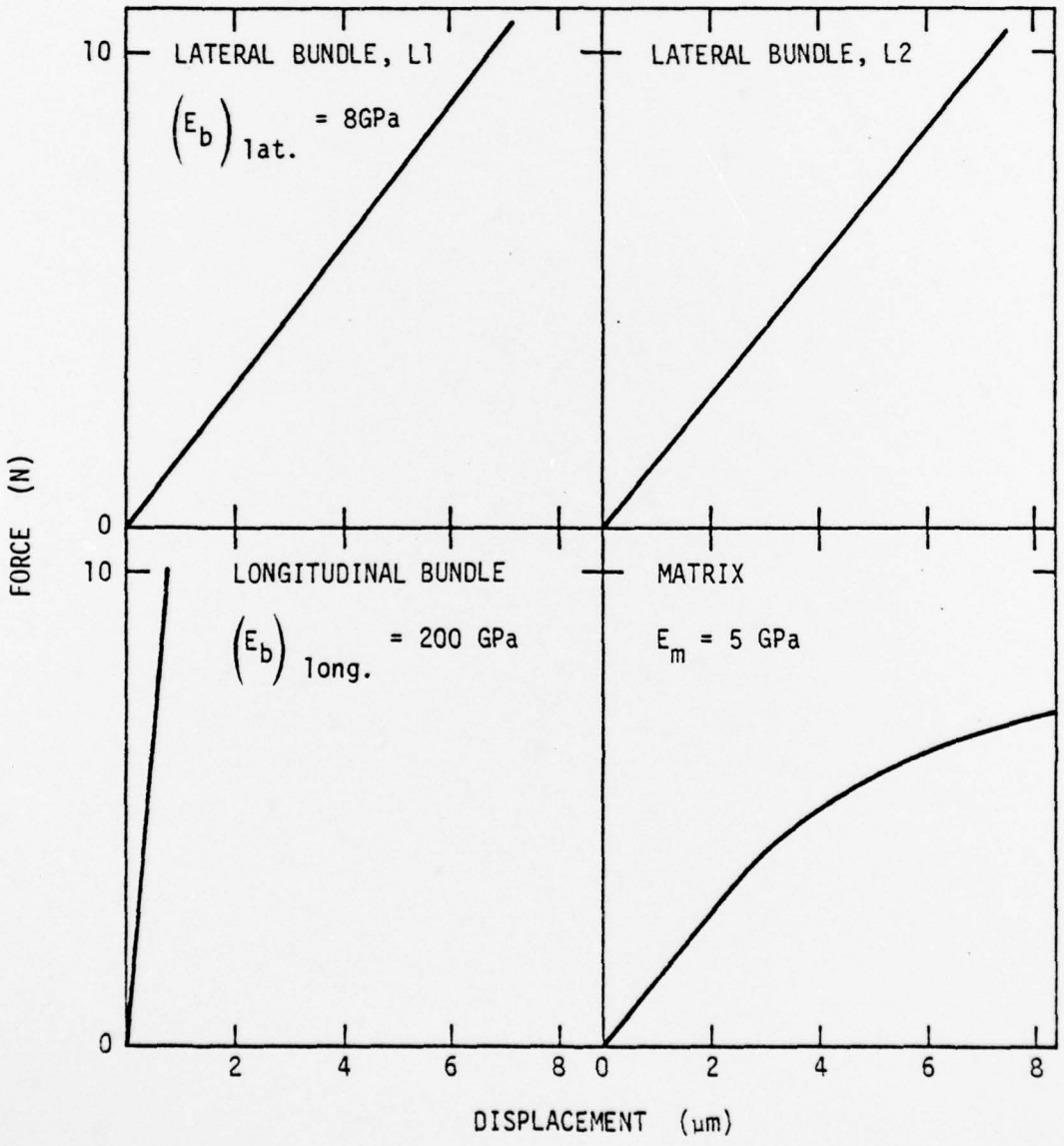
LATERAL BUNDLE, L1
$(E_b)_{lat.}$ = 8GPa
LATERAL BUNDLE, L2
LONGITUDINAL BUNDLE
$(E_b)_{long.}$ = 200 GPa
MATRIX
E_m = 5 GPa
FORCE (N)
10
0
2
4
6
8
DISPLACEMENT (μm)

Figure 11

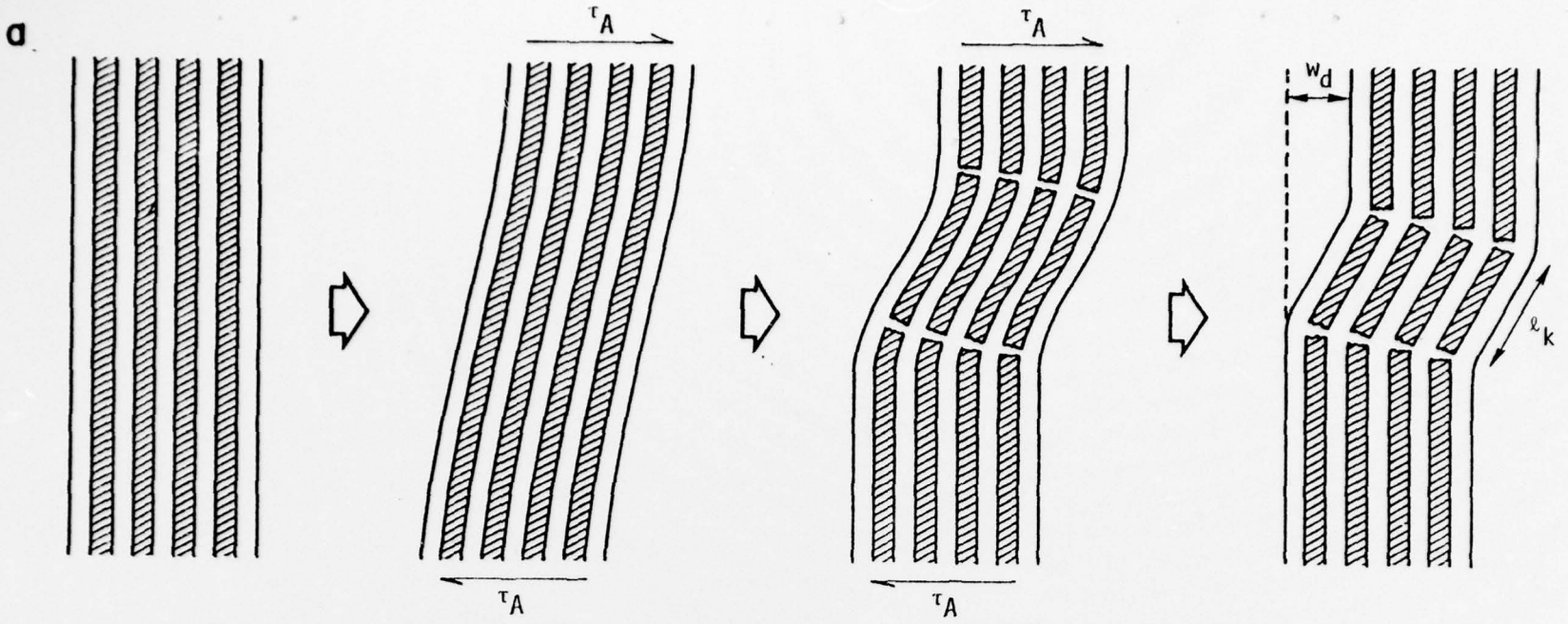
a
τ_A
τ_A
τ_A
τ_A
w_d
ℓ_k

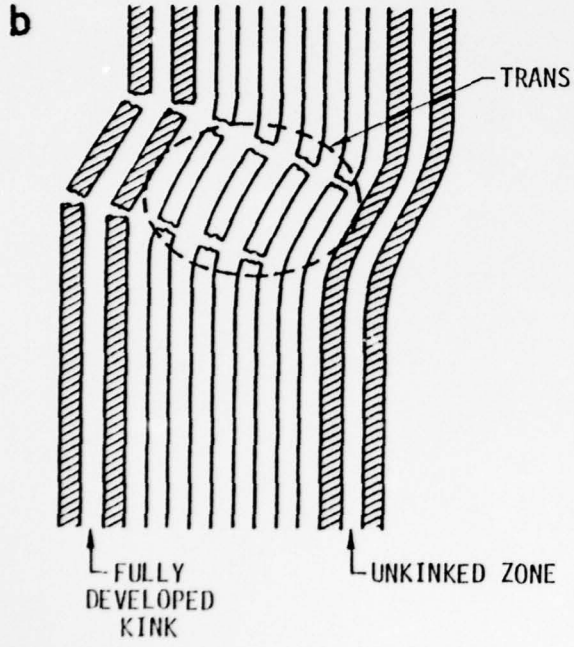
b
TRANSITION ZONE
FULLY DEVELOPED KINK
UNKINKED ZONE

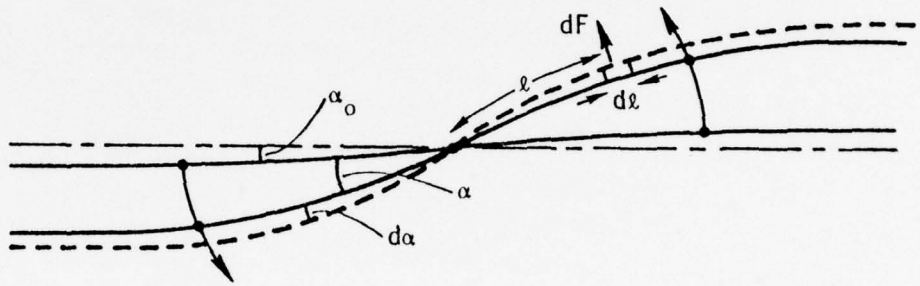
c
dF
ℓ
$d\ell$
α_o
α
$d\alpha$

Figure 12

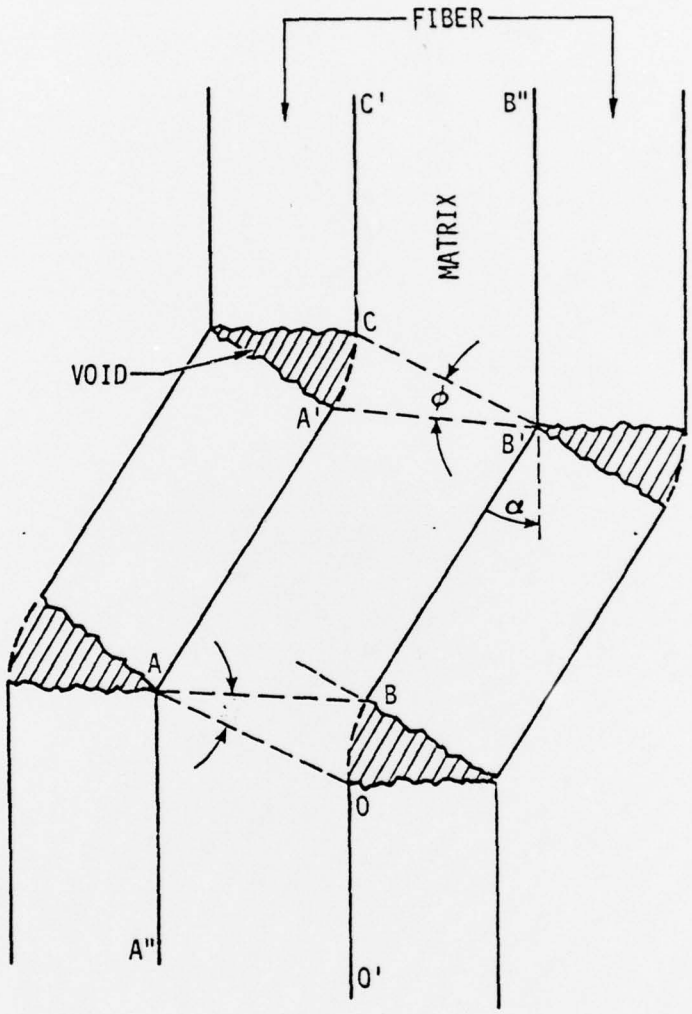

Figure 13

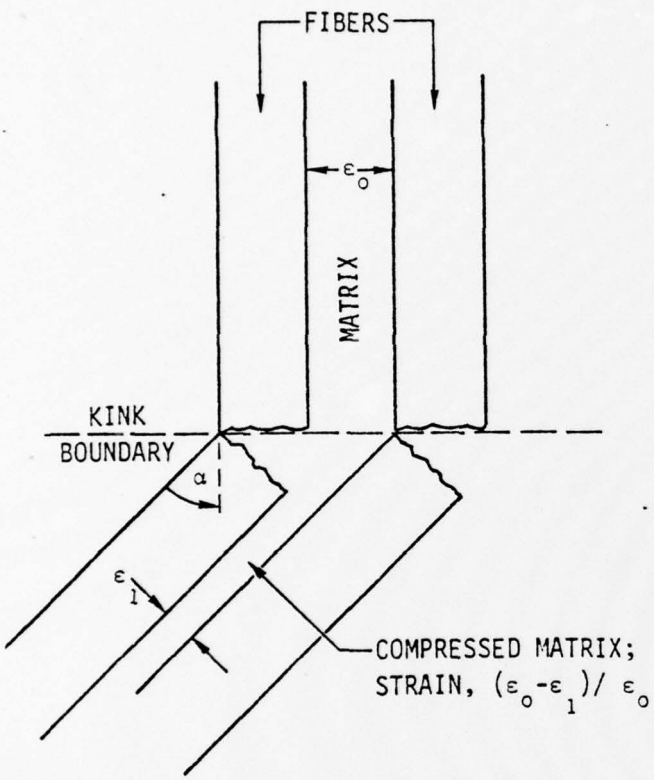

SMALL BOUNDARY INCLINATION

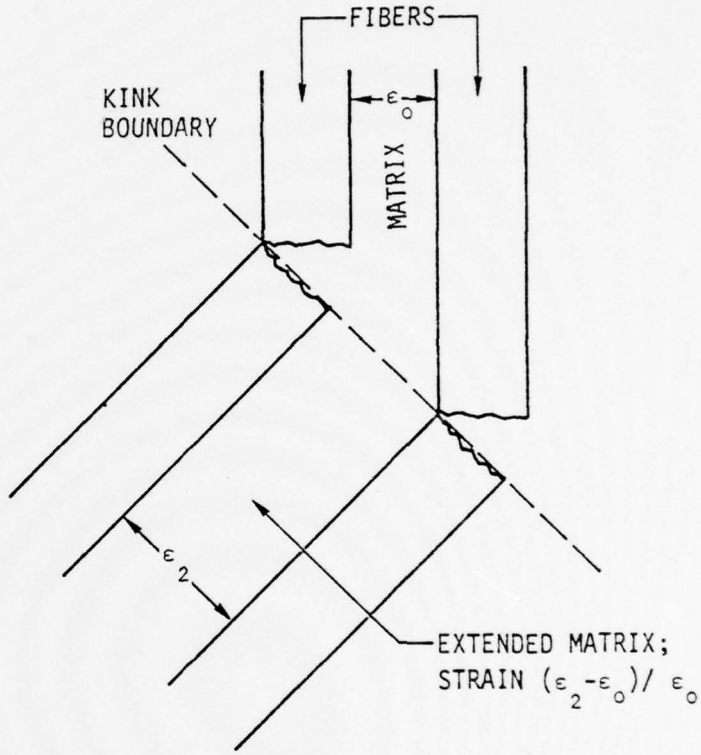

LARGE BOUNDARY INCLINATION

Figure 13b

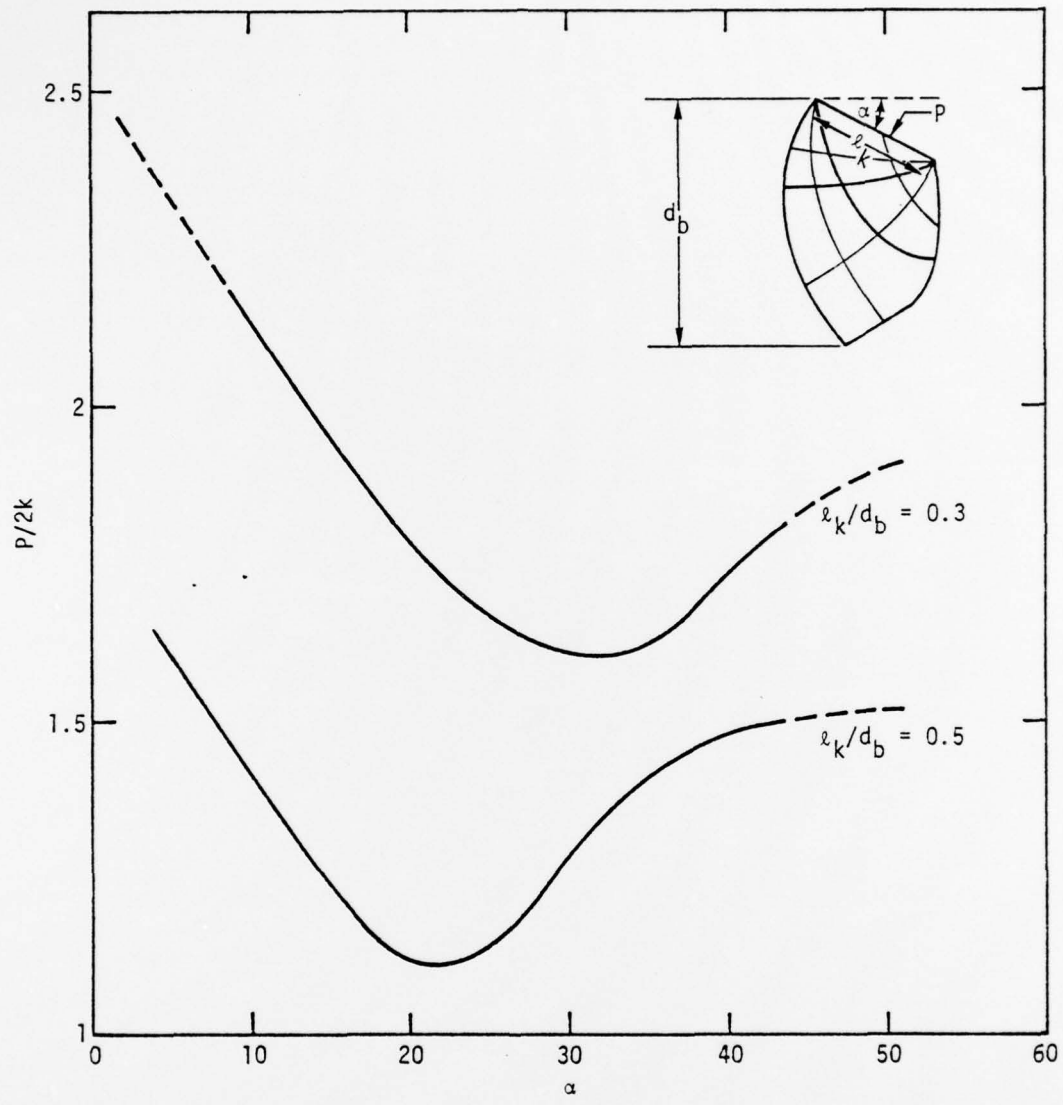

Figure 14

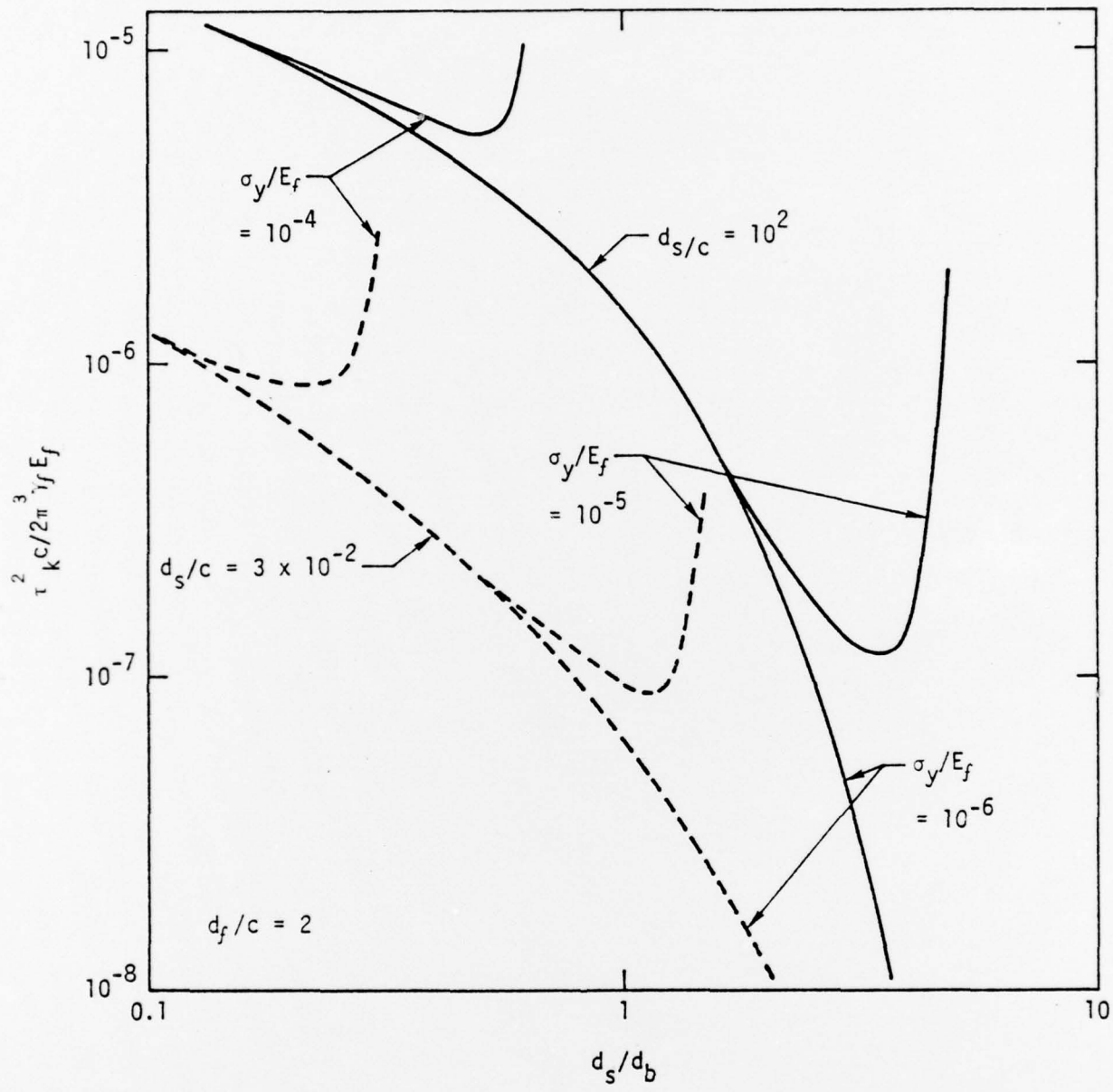
10^{-5}
10^{-6}
10^{-7}
10^{-8}
σ_y/E_f
$= 10^{-4}$
$d_{s/c} = 10^2$
σ_y/E_f
$= 10^{-5}$
$d_s/c = 3 \times 10^{-2}$
σ_y/E_f
$= 10^{-6}$
$d_f/c = 2$
$\tau_k^2 c/2\pi^3 \nu_f E_f$
0.1
1
10
d_s/d_b

Figure 15

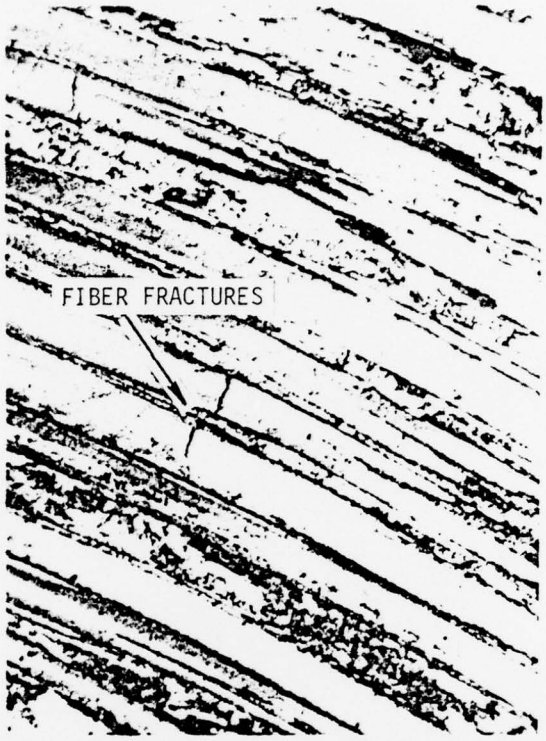

Figure 16

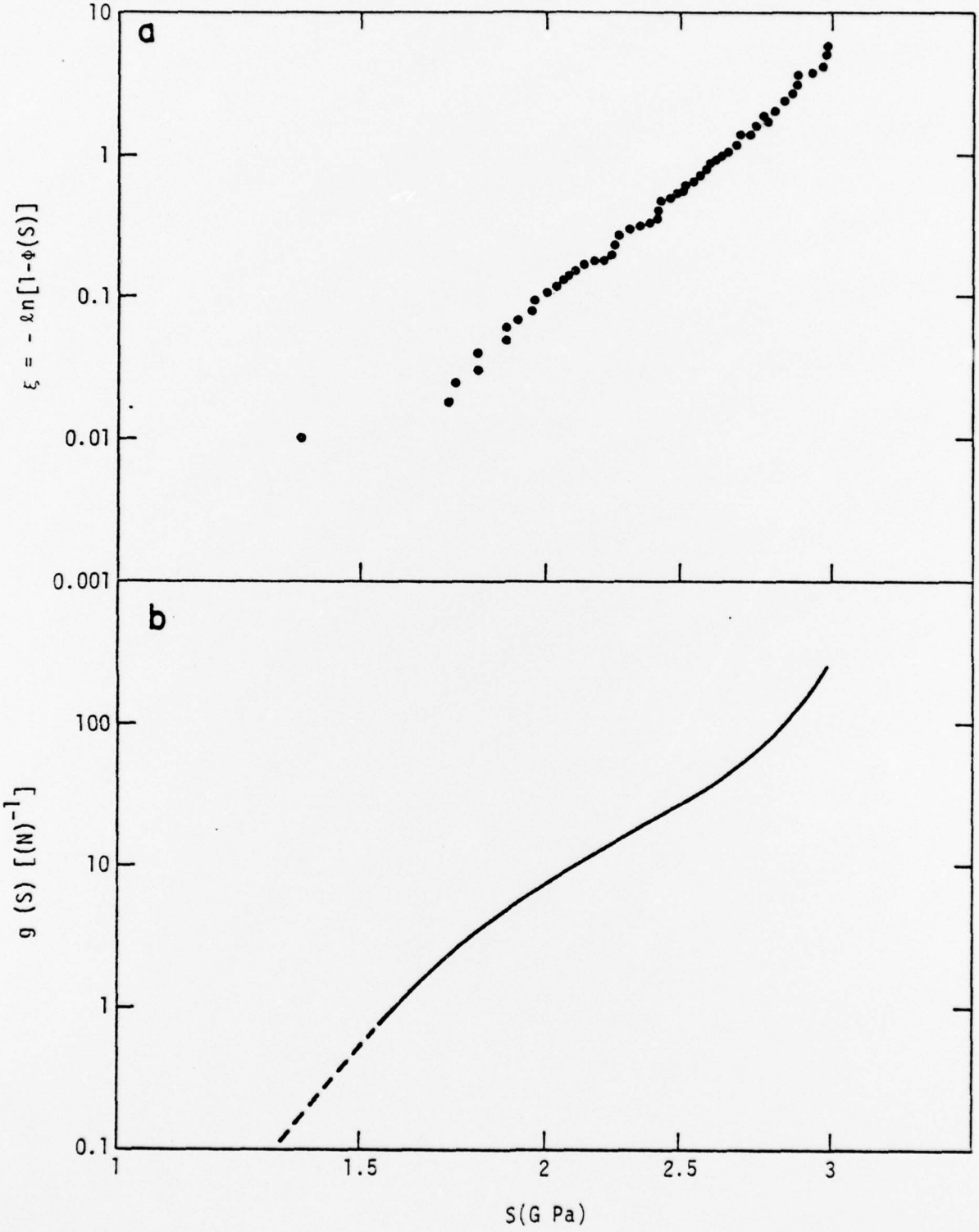

Figure 17

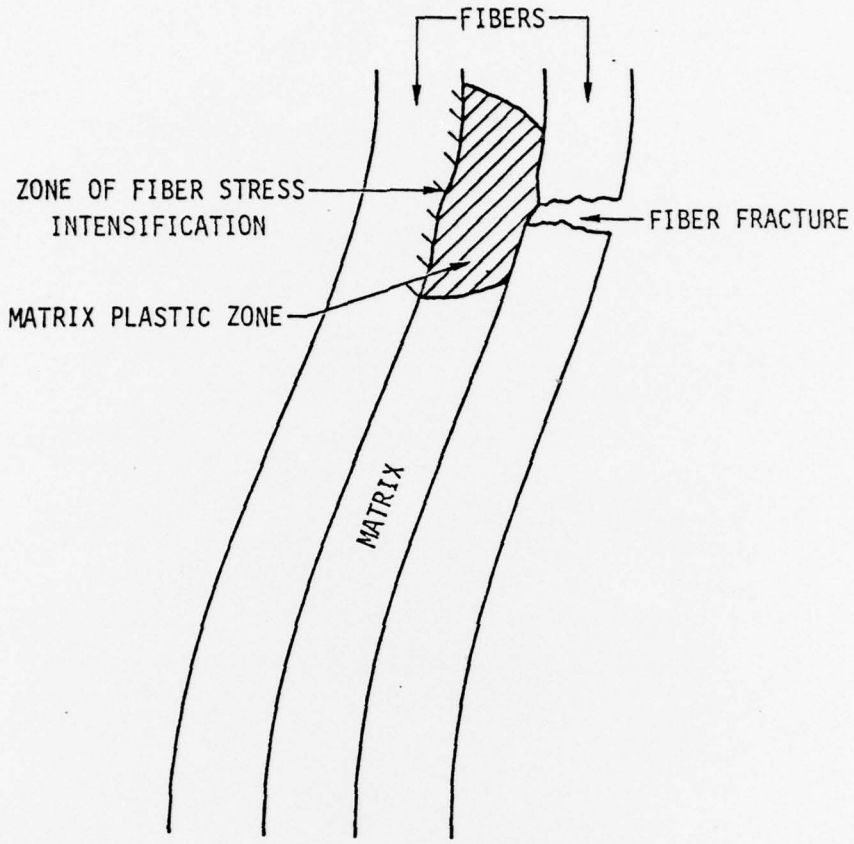
FIBERS
ZONE OF FIBER STRESS INTENSIFICATION
FIBER FRACTURE
MATRIX PLASTIC ZONE
MATRIX

Figure 18

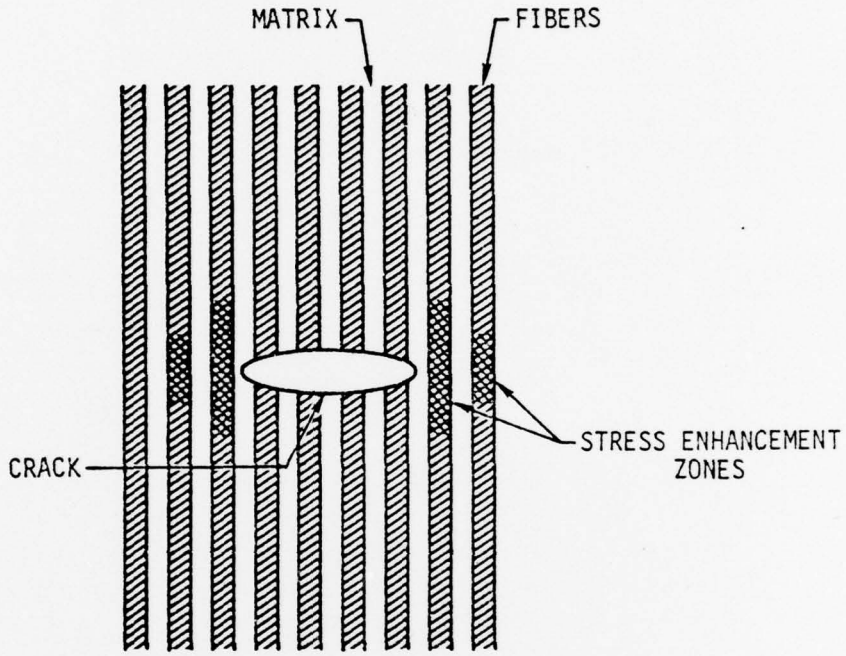

Figure 19

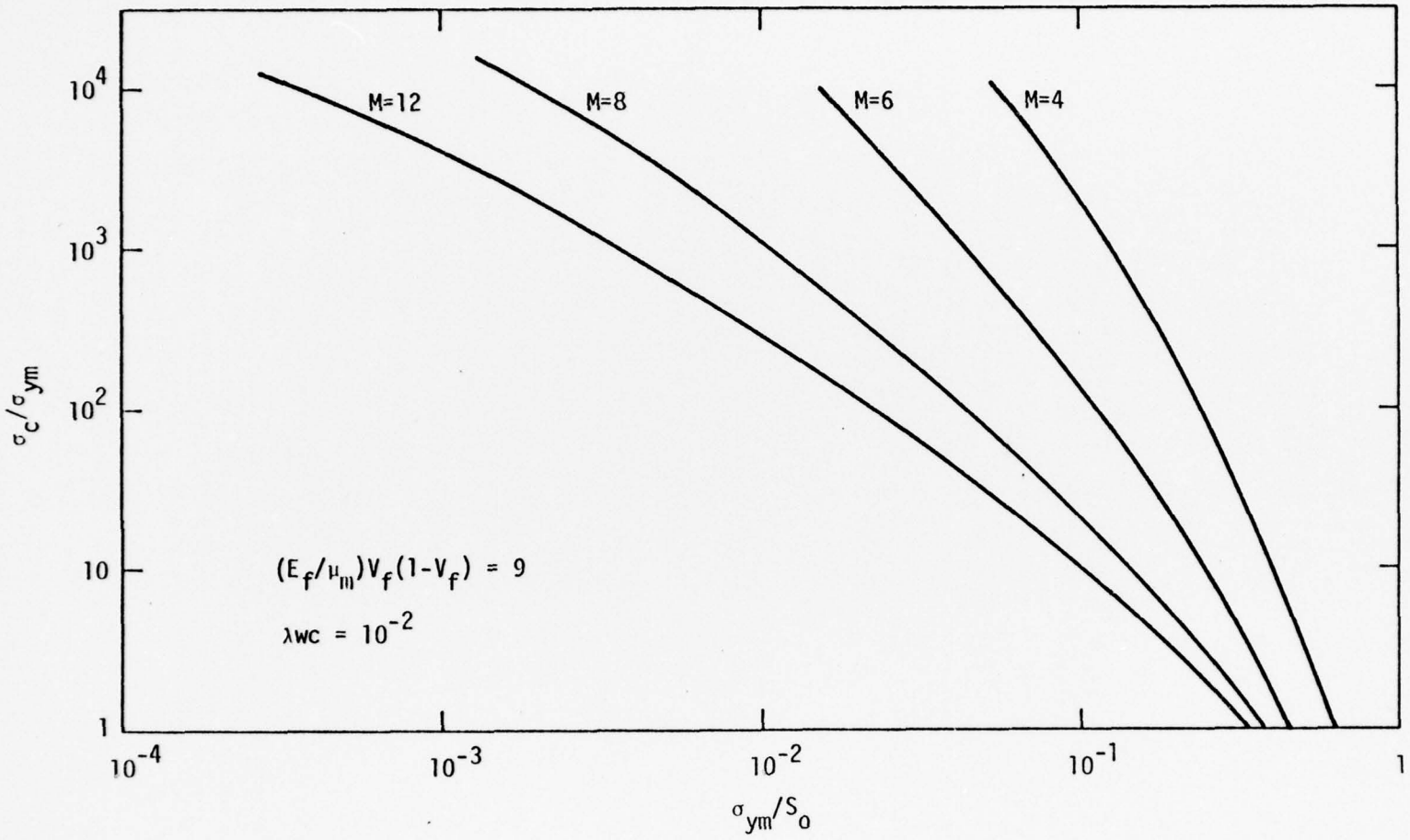
M=12
M=8
M=6
M=4
$(E_f/\mu_m)V_f(1-V_f) = 9$
$\lambda wc = 10^{-2}$
σ_c/σ_{ym}
σ_{ym}/S_o
10^4
10^3
10^2
10
1
10^{-4}
10^{-3}
10^{-2}
10^{-1}
1

Figure 20

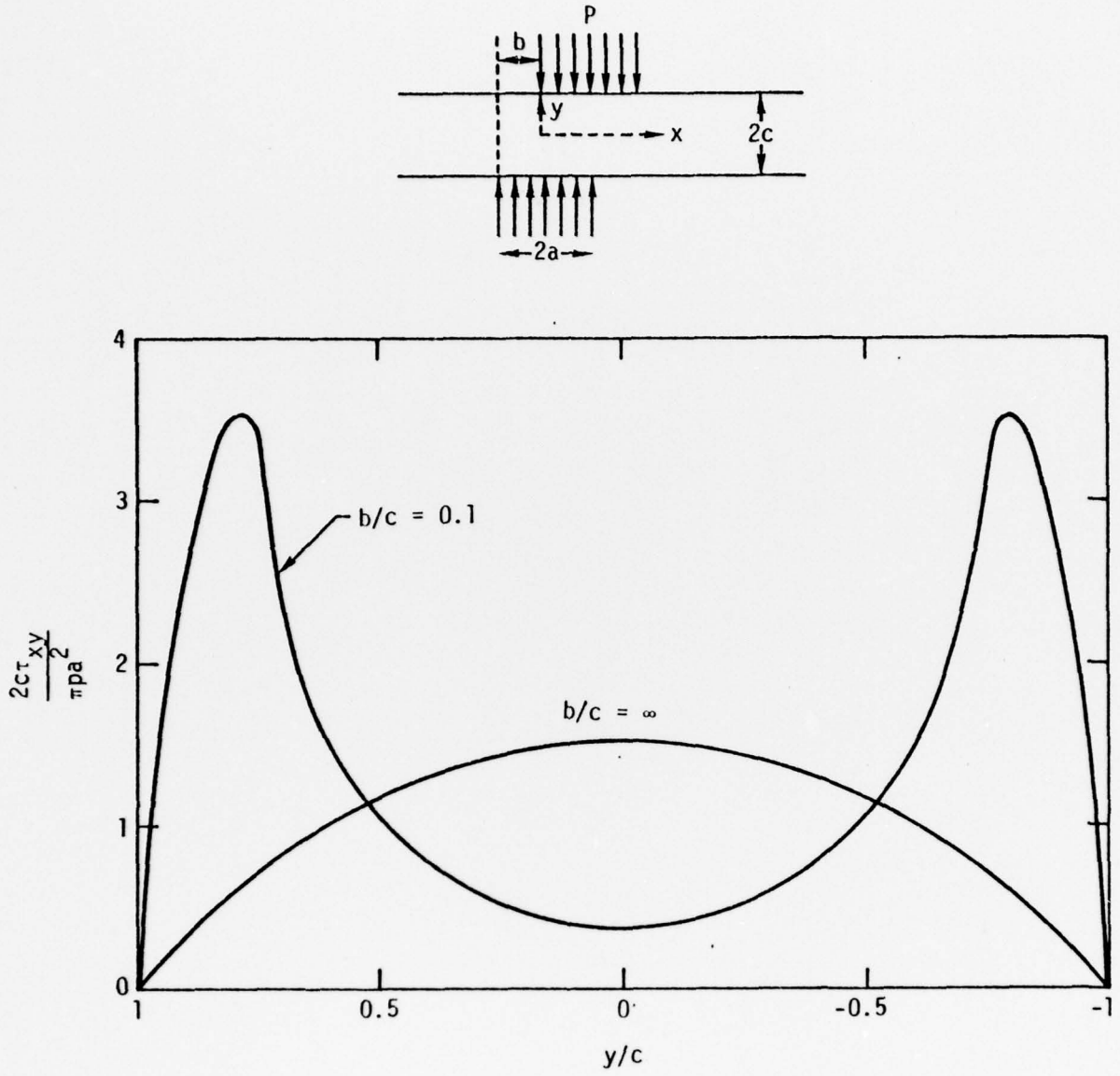

Figure 21

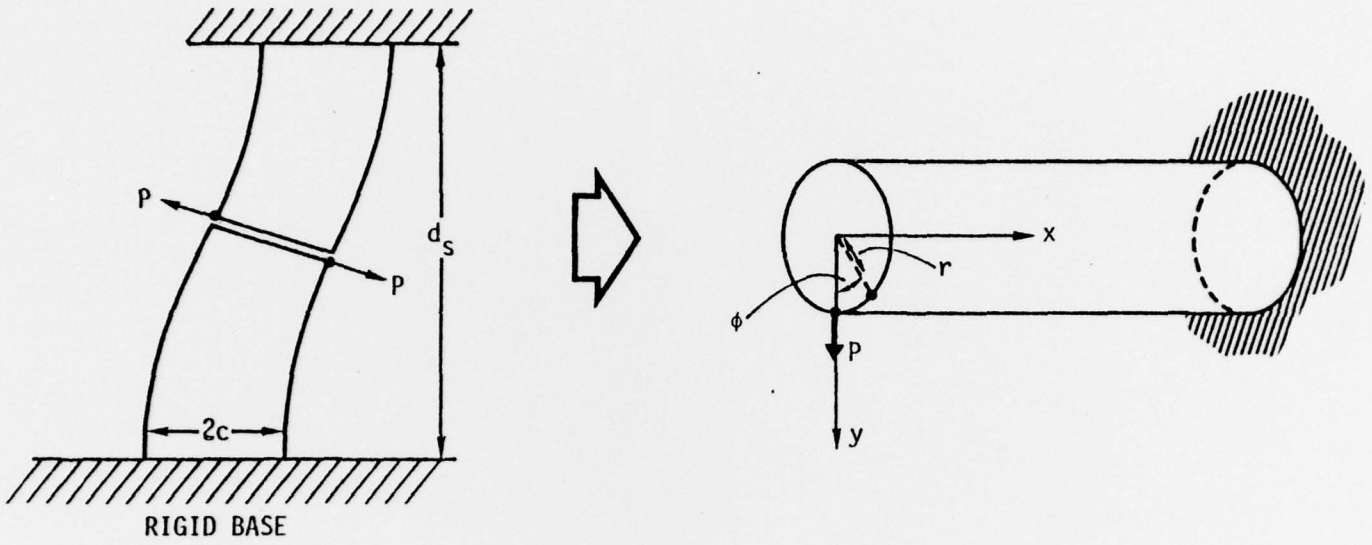

Figure 22